Article

Cell Reports

Two Distinct E2F Transcriptional Modules Drive Cell Cycles and Differentiation

Graphical Abstract

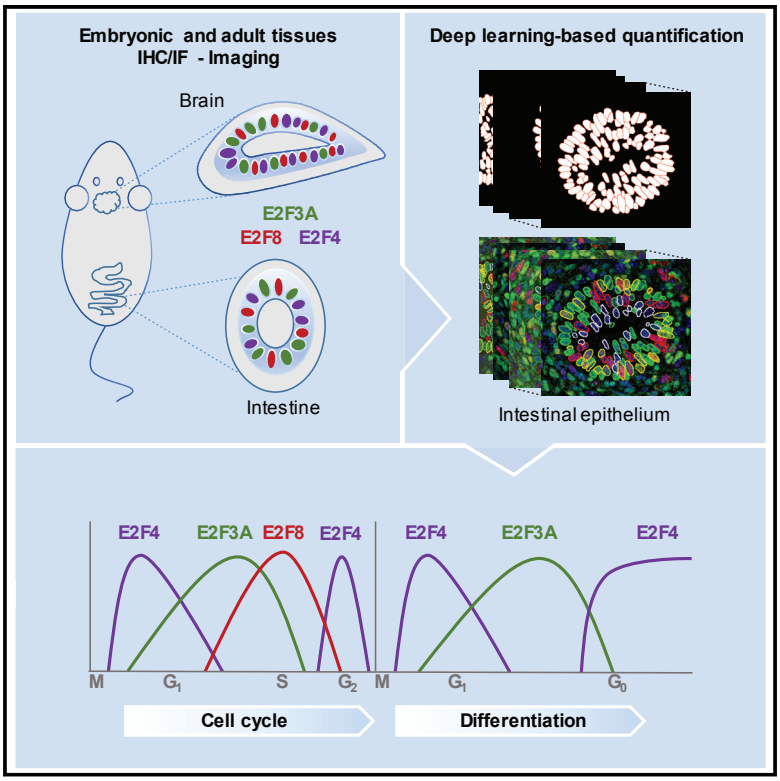

Authors

Maria C. Cuitiño, Thierry Pécot, Daokun Sun, ..., Michael C. Ostrowski, Michele Pagano, Gustavo Leone

Correspondence

leoneg@musc.edu

In Brief

The study of E2Fs *in vivo* has been challenging. Cuitiño et al. reconstruct the spatiotemporal expression of E2F activators (E2F3A) and canonical (E2F4) and atypical (E2F8) repressors during the mammalian cell cycle and propose that orchestrated accumulation of different E2F combinations control gene expression in proliferating (E2F3A-8-4) and differentiating (E2F3A-4) cells.

Highlights

- E2F expression during cell division, differentiation, and quiescence is measured *in vivo*
- E2F3A, E2F8, and E2F4 accumulate sequentially in the nucleus of cycling cells
- E2F3A-4 nuclear accumulation controls gene expression during cell-cycle exit
- Deep learning tools are applied to nuclear segmentation of complex mammalian tissues

Cuitiño et al., 2019, Cell Reports *27*, 1–14
June 18, 2019
https://doi.org/10.1016/j.celrep.2019.05.004

CellPress

Please cite this article in press as: Cuitiño et al., Two Distinct E2F Transcriptional Modules Drive Cell Cycles and Differentiation, Cell Reports (2019), https://doi.org/10.1016/j.celrep.2019.05.004

Cell Reports
Article

Two Distinct E2F Transcriptional Modules Drive Cell Cycles and Differentiation

Maria C. Cuitiño,[1] Thierry Pécot,[1] Daokun Sun,[1,2] Raleigh Kladney,[2] Takayuki Okano-Uchida,[1] Neelam Shinde,[3] Resham Saeed,[3] Antonio J. Perez-Castro,[3] Amy Webb,[4] Tom Liu,[4] Soo In Bae,[2] Linda Clijsters,[5] Nicholas Selner,[1] Vincenzo Coppola,[2] Cynthia Timmers,[1,4] Michael C. Ostrowski,[1] Michele Pagano,[5,6] and Gustavo Leone[1,7,*]
[1]Department of Biochemistry and Molecular Biology, Hollings Cancer Center, Medical University of South Carolina, Charleston, SC 29425, USA
[2]Department of Molecular Genetics, Ohio State University, Columbus, OH 43210, USA
[3]Department of Cancer Biology and Genetics, Ohio State University, Columbus, OH 43210, USA
[4]Comprehensive Cancer Center, Ohio State University, Columbus, OH 43210, USA
[5]Department of Biochemistry and Molecular Pharmacology, Perlmutter Cancer Center, New York University School of Medicine, New York, NY 10016, USA
[6]Howard Hughes Medical Institute, New York University School of Medicine, New York, NY 10016, USA
[7]Lead Contact
*Correspondence: leoneg@musc.edu
https://doi.org/10.1016/j.celrep.2019.05.004

SUMMARY

Orchestrating cell-cycle-dependent mRNA oscillations is critical to cell proliferation in multicellular organisms. Even though our understanding of cell-cycle-regulated transcription has improved significantly over the last three decades, the mechanisms remain untested *in vivo*. Unbiased transcriptomic profiling of G_0, G_1-S, and S-G_2-M sorted cells from FUCCI mouse embryos suggested a central role for E2Fs in the control of cell-cycle-dependent gene expression. The analysis of gene expression and E2F-tagged knockin mice with tissue imaging and deep-learning tools suggested that post-transcriptional mechanisms universally coordinate the nuclear accumulation of E2F activators (E2F3A) and canonical (E2F4) and atypical (E2F8) repressors during the cell cycle *in vivo*. In summary, we mapped the spatiotemporal expression of sentinel E2F activators and canonical and atypical repressors at the single-cell level *in vivo* and propose that two distinct E2F modules relay the control of gene expression in cells actively cycling (E2F3A-8-4) and exiting the cycle (E2F3A-4) during mammalian development.

INTRODUCTION

Cell proliferation and cell differentiation are precisely coordinated during organogenesis, tissue homeostasis, and tissue repair in worms, flies, and other multicellular organisms. Alterations of cell-cycle regulatory components can lead to disease syndromes, including cancer (Cordon-Cardo, 1995; Otto and Sicinski, 2017; Sherr, 1996; Viatour and Sage, 2011). Studies in *C. elegans*, *Drosophila*, *Xenopus*, and a variety of mammalian cell culture systems identified evolutionary conserved signaling pathways that control cell-cycle transitions (Cross et al., 2011). Growth-factor-mediated engagement of cognate receptors invariably culminates in activation of a signaling cascade involving the CDK-RB axis and downstream family of E2F transcription factors (Harbour and Dean, 2000; Korenjak et al., 2004; Nevins et al., 1997). The role of E2F in regulating G_1/S cell-cycle transcription and growth-factor-dependent commitment of cells to enter the cell cycle is well established. Studies using model organisms and cell lines have yielded a detailed understanding of the role of the various E2F family members in regulating E2F-dependent transcription (Bertoli et al., 2013; Chen et al., 2009; Henley and Dick, 2012; Sadasivam and DeCaprio, 2013). However, much less is known about how E2F-dependent transcription is regulated *in vivo*, where a wide range of different cell types and states of differentiation exist.

Whereas flies and worms have either two or three E2Fs, respectively, mammals have eight distinct genes that give rise to at least nine different E2F proteins with transcriptional activation and repression function. Based on structure and function, mammalian E2Fs are further categorized into three subclasses: canonical activators (E2F1-3A/B), canonical repressors (E2F4-6), and atypical repressors (E2F7-8) (Chen et al., 2009; Iaquinta and Lees, 2007; Lammens et al., 2009; Logan et al., 2005). Canonical activators associate with coactivator proteins to robustly induce RNA-polymerase-II-dependent gene expression (Danielian et al., 2008; Trimarchi and Lees, 2002). Canonical repressors respond to CDK signaling and recruit histone deacetylases (HDACs), polycomb group proteins, Mga, and Max to E2F target promoters (Attwooll et al., 2004). Canonical activators and repressors bind target promoter sequences through a single DNA-binding domain, require physical association with dimerization partner (DP) proteins (Chen et al., 2009; DeGregori and Johnson, 2006; Magae et al., 1996), and physically associate with RB and related pocket proteins (Ginsberg et al., 1994; Lees et al., 1993; Leone et al., 1998). Atypical repressors bind DNA target sequences through two DNA-binding domains and function independent of DP and pocket protein physical interactions (Christensen et al., 2005; Di Stefano et al., 2003; Logan et al., 2005; Maiti et al., 2005).

Please cite this article in press as: Cuitiño et al., Two Distinct E2F Transcriptional Modules Drive Cell Cycles and Differentiation, Cell Reports (2019), https://doi.org/10.1016/j.celrep.2019.05.004

Why mammals evolved to have multiple E2F activator and repressor proteins remains a mystery. Collectively, all E2Fs share the ability to bind and control the same regulatory sequences on target promoters, yet single E2F knockout mice manifest pathological phenotypes in distinct organs and at different developmental stages, suggesting that each E2F may have unique roles and functions during development (Field et al., 1996; Humbert et al., 2000a, 2000b; Lindeman et al., 1998; Murga et al., 2001; Rempel et al., 2000). Combinatory knockout mice lacking multiple E2Fs within each subclass, however, generally have distinct or more pronounced phenotypes in a broader set of organs and earlier in development, suggesting significant functional redundancy (Chen et al., 2009; DeGregori and Johnson, 2006). Understanding how E2F activator and repressor functions are coordinated to regulate a wide spectrum of cellular processes *in vivo* has been hampered by a paucity of fundamental information relating to "when and where" each E2F is expressed. We employed fluorescent ubiquitination-based cell-cycle indicator (FUCCI) mice and flow cytometry cell sorting coupled to RNA sequencing and generated tagged E2F knockin mice as well as imaging and deep learning quantification tools to comprehensively map the temporal and spatial expression of representative activator (E2F3A) and canonical (E2F4) and atypical repressor (E2F8) E2F proteins during embryonic and adult development. These three sentinel E2Fs have been shown to play particularly important roles in mouse development (Humbert et al., 2000a; Li et al., 2008; Rempel et al., 2000; Tsai et al., 2008). Our observations expose two distinct exquisitely regulated E2F transcriptional modules that differ by the repressor proteins utilized. One module (E2F3A-8-4) controls cell-cycle-dependent gene expression in actively cycling cells, and the other module (E2F3A-4) controls gene expression in cells programmed to exit the cell cycle. Remarkably, these two transcriptional modules operate similarly in all tissues of the mouse, exposing a universal mechanism for mitotic cell cycle regulation in mammals.

RESULTS

FUCCI Embryos Identify E2Fs as Key Drivers of Cell-Cycle-Dependent Transcriptomic Profiles

We used FUCCI bi-transgenic mice (*mKO2-hCDT1;mAG-hGEM*) (Sakaue-Sawano et al., 2008) to isolate embryonic cells at different stages of the cell cycle and gain insight into cell-cycle-regulated transcription *in vivo*. Expression of Kusabira-orange-tagged CDT1 (mKO2-hCDT1) and Azami-green-tagged GEMININ (mAG-hGEM) proteins allow different phases of the cell cycle to be identified *in vivo* by virtue of their distinct cell-cycle-dependent protein stabilities and fluorescent properties. Accumulation of mKO2-hCDT1 protein is maximum in G_0 (bright red), intermediate in G_1 and early-mid S phase (dim red), and not detectable in late S and G_2-M. In contrast, mAG-hGEM (green) accumulates throughout S-G_2-M, with no detectable protein in G_0 and G_1. The concomitant accumulation of both reporter proteins in early-mid S phase endows cells with yellow fluorescence. With these genetic tools on hand, timed pregnancies were set and bi-transgenic *mKO2-hCDT1;mAG-hGEM* embryos were collected at embryonic days 10.5 (E10.5), E11.5, and E13.5 post-coitus. Embryos were dissociated into single cells and separated by fluorescence-activated cell sorting (FACS). Using wild-type and single transgenic mice to accurately calibrate sorting of cells based on their fluorescence spectrum, G_0 (bright red), G_1 (dim red), G_1-S (yellow), and S-G_2-M (green) cell populations were collected (Figures S1A and S1B). All sorted samples, along with unsorted (US) control cells, were subjected to whole-transcriptome gene profiling by RNA sequencing (RNA-seq). After mapping reads to the genome using an adapted standard pipeline (see STAR Methods), RNA profiles were compared. Correlation analysis showed that cell-cycle phase-specific profiles from different same-age embryos were nearly identical (R = 0.998; Figure S1C), whereas principal-component analysis illustrated significant differences in gene expression between them (Figure 1A). The cell-cycle-dependent expression of a well-characterized set of genes confirmed the cell-cycle phase assignment based on mKO2-hCDT1 and mAG-hGEM protein accumulation and FACS (Figure 1B). Real-time qPCR analysis of the same gene set confirmed the impressive log-fold gene expression changes among cell-cycle fractions measured by RNA-seq (Figure 1B). Together, these analyses validated the robustness of combining the FUCCI system with FACS to assess cell-cycle phase-specific global gene expression profiles *in vivo*.

We next compared expression profiles derived from cycling cells (G_1, G_1-S and S-G_2-M) relative to quiescent cells (G_0) (Figures 1C and S1D; Table S1). Genes consistently expressed >2 log-fold higher (with an adjusted p value < 0.05) in G_1, G_1-S or S-G_2-M samples than in G_0 samples across all three embryonic ages were denoted proliferation related. Of these 258 proliferation-related genes, 86 were previously reported as periodically expressed during the cell cycle (Figure S1F) (Santos et al., 2015). The majority of genes expressed higher in G_0 samples than in G_1, G_1-S, or S-G_2-M samples (267 genes) were related to cell differentiation and non-proliferative processes and denoted as quiescence related. Analysis of these two gene classes revealed a remarkable enrichment of E2F-binding consensus sequences near the transcriptional start site of proliferation-related promoters, with seven of the top ten transcription factors predicted to bind to promoter regions of proliferation-related genes having E2F-binding consensus sites and enrichment of a variety of other transcription factor binding sequences in quiescent-related promoters (Figure 1D). Integration of our RNA-seq results with previously published chromatin immunoprecipitation (ChIP) experiments indicated the recruitment of E2F family members to the vast majority (75%) of proliferation-related promoters (Figures 1C and S1D) (Kent et al., 2016, 2017; Oki et al., 2018; Santos et al., 2015; Westendorp et al., 2012). Together, these unbiased transcriptomic analyses of "cell-cycle-phase-specific" sorted embryonic cells suggested a central involvement for E2F family members in the control of cell-cycle-dependent gene expression *in vivo*.

Development of Specific Reagents to Measure E2F3A, E2F4, and E2F8 Proteins *In Vivo*

The oscillatory nature of cell-cycle-regulated gene expression has been proposed to result, at least in part, from sequential waves of E2F mediated transcriptional activation and repression (Giangrande et al., 2004; Li et al., 2008). In agreement with measurements made in cell culture systems, *E2f1-3a* and *E2f7-8* mRNA levels increased in G_1 cells when compared to cells in

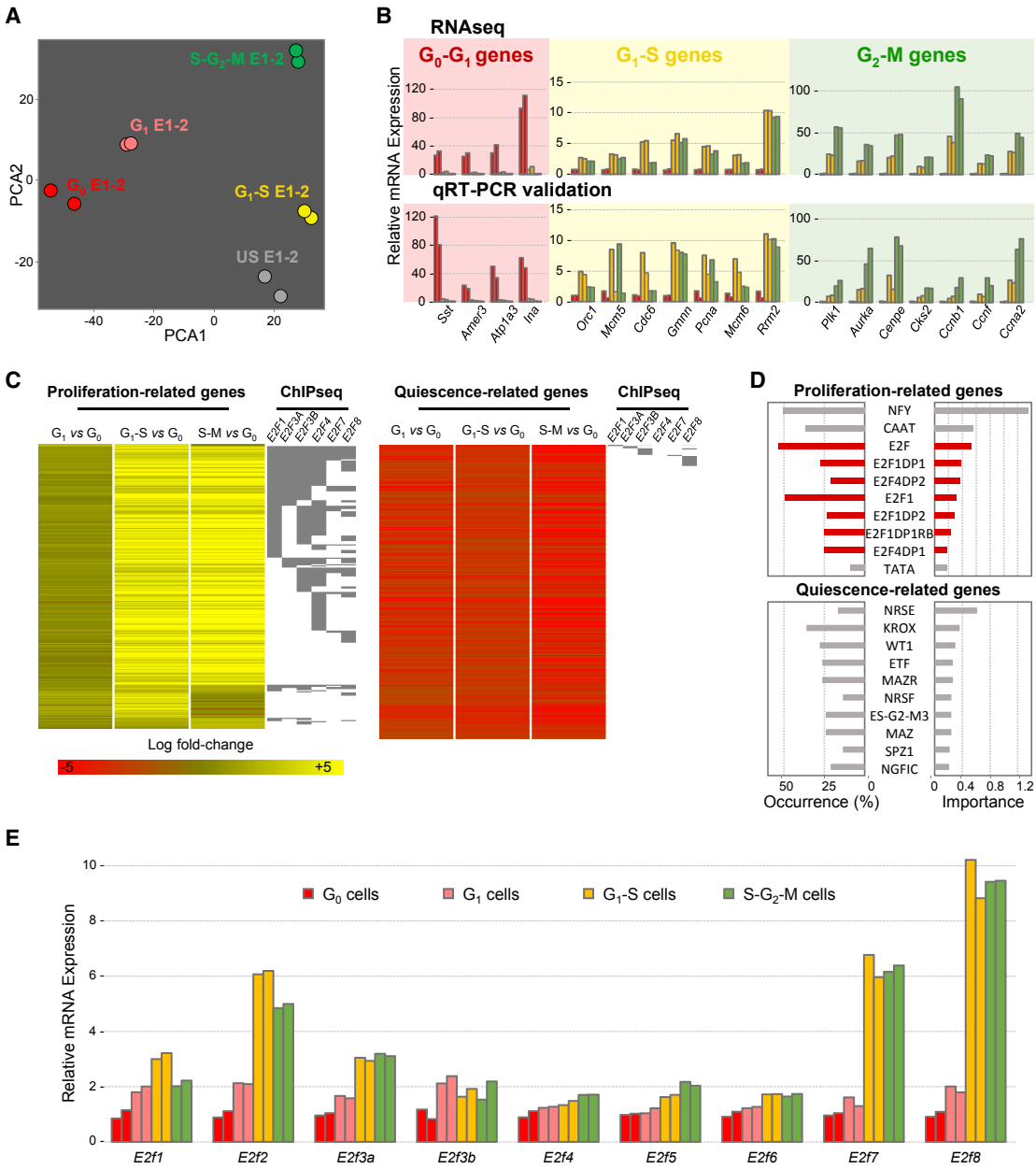

Figure 1. *In Vivo* Analysis of Cell-Cycle-Dependent mRNA Profiles

(A) Principal-component analysis of levels of gene expression, as measured by RNA-seq, of two replicates of the G_0, G_1, G_1-S, S-G_2-M, and US cell populations from bi-transgenic (mKO2-hCDT1;mAG-hGEM) FUCCI embryos at embryonic day 13.5 (E13.5). US, unsorted.

(B) Expression analysis of cell cycle genes in the FUCCI cell populations. Fold changes are relative to S-G_2-M for the G_0-G_1 genes and G_0 for the G_1-S and G_2-M genes. Top: RNA-seq. Bottom: real-time qPCR. Each bar represents sorted cells from an E13.5 FUCCI embryo from an independent experiment.

(C) Heatmaps of the log2 fold-change values for differentially expressed genes in the cycling (G_1, G_1-S, and S-G_2-M) and quiescent (G_0) cell populations at E13.5 (n = 2 embryos). E2F target genes as identified by chromatin immunoprecipitation (ChIP) experiments are indicated on the right of each heatmap.

(D) Top 10 transcription factors estimated to bind to the evolutionary conserved 5′ UTR and promoter regions of the proliferation- and quiescence-related genes using distant regulatory elements (DiRE; see STAR Methods).

(E) Gene expression analysis of E2F family members in the FUCCI cell populations. Fold changes, as measured by RNA-seq, are relative to G_0. Each bar represents an E13.5 FUCCI embryo from an independent experiment.

See also Figure S1 and Table S1.

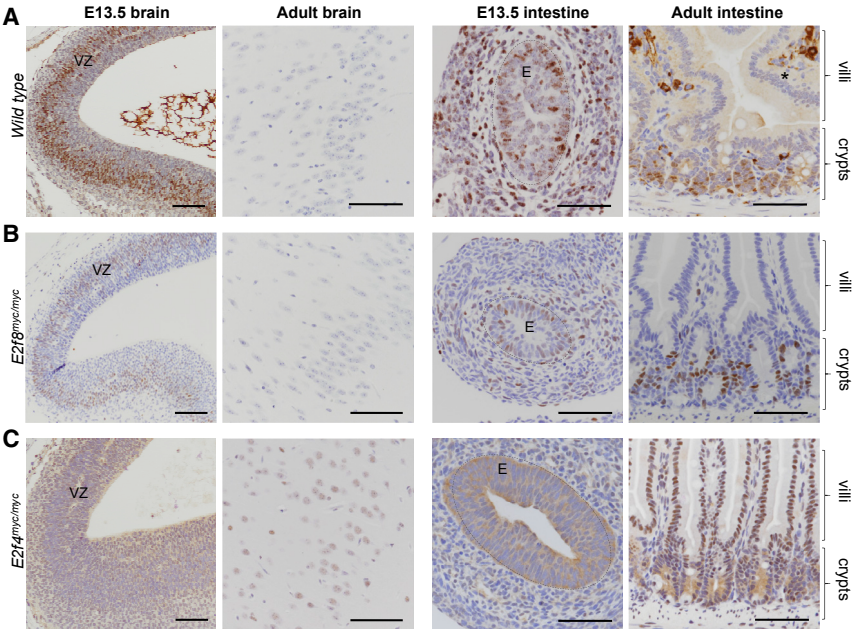

Figure 2. Expression of E2F3A, E2F8, and E2F4 in Proliferative and Quiescent Tissues

(A) E2F3A immunohistochemistry (IHC) on tissues of wild-type mice. E13.5 and adult brain (left two panels); E13.5 and adult intestine (right two panels). Note the nonspecific cytoplasmic staining of interstitial cells (asterisk).

(B) E2F8 IHC on tissues of *E2f8*$^{myc/myc}$ mice. E13.5 and adult brain (left two panels); E13.5 and adult intestine (right two panels).

(C) E2F4 IHC on tissues of *E2f4*$^{myc/myc}$ mice. E13.5 and adult brain (left two panels); E13.5 and adult intestine (right two panels).

E2F8 and E2F4 were detected using MYC antibody. Tissues were counterstained with hematoxylin. VZ, ventricular zone; E, epithelium. Scale bars, 200 μm. See also Figures S2–S5.

G_0, with maximum levels found in S and G_2, and the mRNA levels of *E2f3b*, *E2f4*, *E2f5*, and *E2f6* remained relatively unchanged across all cell-cycle phases (Figures 1E and S1E). These observations suggest that transcriptional regulation might be important for the timely induction of *E2f1-3a* and *E2f7-8* mRNA levels *in vivo*. However, the simultaneous accumulation of these activator and repressor E2F mRNAs suggests that additional post-transcriptional mechanisms are likely involved in regulating sequential waves of coordinated E2F-mediated activation and repression during the cell cycle.

Because transcript levels may not reflect protein levels, we proceeded to examine the spatial and temporal distribution of representative E2F activator (E2F3A), canonical repressor (E2F4), and atypical repressor (E2F8) proteins *in vivo*. These three sentinel E2Fs, where E2F3A is similar to E2F1 and E2F2, E2F4 is similar to E2F5, and E2F8 is similar to E2F6 and E2F7, play particularly important roles in mouse development (Humbert et al., 2000a; Li et al., 2008; Rempel et al., 2000; Tsai et al., 2008). To this end, we used tissues from wild-type and *E2f3a*$^{-/-}$ knockout mice to first validate the specificity of a commercially available monoclonal antibody developed against the E2F3A activator, which has a distinct 121 N-terminal amino acids from the closely related E2F3B isoform (Figures S2A and S2B) (Adams et al., 2000; Leone et al., 2000). Because high-quality specific antibodies against canonical and atypical E2F repressors suitable for immunohistochemistry (IHC) are unavailable, we used homologous recombination in mice to target the expression of a 5x-MYC (human) tag fused to the N termini of canonical (E2F4) and atypical (E2F8) repressor proteins, from their respective endogenous loci (Figures S2C and S2D). Southern blot and PCR genotyping confirmed correct targeting of mouse ESCs, generation of chimeric offspring, and germline transmission of the targeted *E2f4*^{myc} and *E2f8*^{myc} alleles (Figures S2E–S2H). Western blotting of protein lysates from *E2f4*$^{myc/+}$ and *E2f8*$^{myc/+}$ embryos using MYC tag and E2F-specific antibodies confirmed equivalent levels of MYC-tagged E2F4 and E2F8 proteins relative to their non-tagged counterparts (Figures S2I and S2J). Moreover, IHC analysis of tissue sections from wild-type, *E2F4*$^{myc/myc}$, and *E2f8*$^{myc/myc}$ mice confirmed robust and specific detection of MYC-tagged E2F4 and E2F8 proteins using anti-human MYC antibodies (Figures S2K and S2L). Finally, we assessed whether the MYC tag might interfere with normal functions of these two E2Fs. Previous work showed that ablation of *E2f4* in mice results in perinatal lethality (Humbert et al., 2000a; Rempel et al., 2000) and that the combined loss of *E2f7* and *E2f8*, but not loss of either atypical repressor alone, results in embryonic lethality (Li et al., 2008). Interbreeding *E2f4*$^{myc/+}$ mice yielded Mendelian ratios of viable, healthy, and fertile *E2f4*$^{myc/myc}$ mice (Figures S2M and S2N). Similarly, interbreeding *E2f8*$^{myc/+}$ and *E2f7*$^{-/-}$ mice yielded Mendelian ratios of viable and healthy *E2f7*$^{-/-}$;*E2f8*$^{myc/myc}$ mice (Figures S2O and S2P). These results suggested that MYC-tagged E2F4 and E2F8 function normally during development. In summary, we developed highly specific reagents to assess E2F protein expression *in vivo* under physiological conditions at the single-cell level.

E2F3A and E2F8 Accumulate in Proliferating Cells

With these reagents in hand, endodermal, ectodermal, and mesodermal derived tissues from embryonic, neonatal, juvenile, and adult wild-type and *E2f8*$^{myc/myc}$ mice were evaluated for the expression of E2F3A and E2F8. When viewed under low magnification, the overall expression of E2F3A and E2F8 was higher in E13.5 embryos than in E18.5 embryos or adult tissues (Figures 2A, 2B, S3A, and S3B). Moreover, their expression was essentially absent in adult tissues where quiescent cells predominate, including the brain and intestinal villi. Inspection of immunostained tissue sections at higher magnification revealed robust periodic nuclear E2F3A and E2F8 expression in proliferative zones, as demarcated by Ki67 positivity (Figure S4A), of all three germ layers of embryonic and adult tissues, including brain, intestine, tooth, stomach, and every other embryonic and adult tissue examined (Figures 2A, 2B, S3A, and S3B). Endocycling

cell types, such as developing cardiomyocytes, urothelial cells, and splenic megakaryocytes, were also strongly stained for E2F3A and E2F8 (Figures S3A and S3B). We also explored undifferentiated and differentiated cell lineages further in the small intestine of mice. Using standard histological analysis and the stem-cell reporter LGR5 mouse, we found that E2F3A and E2F8 are expressed in intestinal stem cells, but not in differentiated Paneth cells (Figures S4A–S4C). While other organ-specific lineages remain to be thoroughly analyzed, these observations suggest E2F3A and E2F8 are also expressed in tissue progenitor cells. In summary, these analyses revealed that nuclear E2F3A and E2F8 accumulate in all proliferating cells, regardless of their differentiation status, throughout embryonic development and adulthood.

Nuclear E2F4 Accumulation Is Periodic in Proliferating Cells and Permanent in Quiescent Cells

A similar analysis of *E2f4*$^{myc/myc}$ embryonic and adult tissues showed that E2F4 protein was uniformly detected throughout embryonic and adult development, with some consistent differences in expression levels between organs (Figures 2C and S5B) and in intracellular localization depending on the proliferative status of cells. E2F4 was uniformly detected in the cytoplasm of cycling cells within highly proliferative tissues, such as in neuronal progenitors in the ventricular zone of E13.5 brains, intestinal epithelium of E13.5 embryos, intestinal intervillus regions of E18.5 embryos, and intestinal crypts of adult mice (Figures 2C and S5B). Within these proliferative tissues, there were also some interspersed proliferating cells displaying nuclear staining. In nonproliferating well-differentiated cells, such as neurons, enterocytes lining intestinal villi, and Paneth cells, E2F4 protein was predominantly nuclear, with little or no detectable protein in the cytoplasm (Figures 2C, S5B, and S4A). Intestinal stem cells displayed either predominantly cytoplasmic or nuclear E2F4 staining (Figure S4A). In summary, these findings suggest that E2F4 is ubiquitously expressed throughout development, but its nuclear localization is periodic in proliferating cells and permanent in quiescent cells.

E2F8 Is Restricted to Proliferating Cells, whereas E2F3A Extends to Cells Exiting the Cell Cycle

The *in vivo* analysis of E2F activators and repressors described above provided a general view of their spatiotemporal patterning, but the complex architectural organization of most tissues precludes the careful evaluation of E2Fs in the context of proliferation and differentiation. Thus, we selected two tissues with unique spatial compartmentalization of cell proliferation and differentiation for further *in vivo* analysis: the lens and epidermis. The neonatal lens is composed of four zones based on their proliferation status as visualized by Ki67 IHC (Figure 3A). Slow-dividing epithelial cells are located within the anterior zone, and rapidly dividing progenitor cells are located in the adjacent germinative zone. In the transition zone, just beyond the lens equator, progenitor cells receive signals to exit the cell cycle and migrate toward the center of the lens (lens cortex), where they become fully differentiated anucleated lens fibers (Mochizuki and Masai, 2014). IHC staining of wild-type neonate lenses showed nuclear E2F3A in alternating cells located within the anterior and germinative zones (Figure 3B). E2F3A was also detected in the transition zone but was absent in fiber precursor cells undergoing terminal differentiation. Nuclear E2F8 expression in *E2f8*$^{myc/myc}$ lenses was restricted to the anterior and germinative zones, with no detectable expression in the transition or cortex zones (Figure 3B). Cytoplasmic E2F4 staining was robust in all epithelial cells within the anterior and germinative zones of *E2f4*$^{myc/myc}$ lenses, decreased in the transition zone, and was undetectable in mature fibers within the cortex (Figure 3B). However, nuclear E2F4 was detected in alternating cells within the anterior, germinative, and transition zones and uniformly detected in differentiating lens fibers prior to becoming anucleated (Figure 3B).

The innermost basal layer of the epidermis is composed of proliferative keratinocytes, which then exit the cell cycle, differentiate, and migrate outwardly to form the spinous, granular, and cornified layers (Figure 3A) (Blanpain and Fuchs, 2006; Byrne and Hardman, 2002). In 1-day-old pups, nuclear E2F3A expression extended from the basal proliferating keratinocytes into the differentiating spinous layer before disappearing in the granular and cornified layers (Figure 3C). Nuclear E2F8 expression was restricted to basal keratinocytes, with no expression in the spinous layer (Figure 3C). Cytoplasmic E2F4 was detected throughout the stratified epithelium, whereas nuclear E2F4 staining was fainter in basal proliferative keratinocytes than in differentiating spinous and granular cell layers (Figure 3C). A similar spatial pattern of E2F3A, E2F8, and E2F4 expression was observed in other stratified squamous epithelia, including the adult non-glandular stomach and small intestine (data not shown). In summary, E2F3A, E2F8, and E2F4 nuclear protein levels oscillate in zones of cell proliferation but have a different pattern of accumulation in differentiating cells. Atypical repressor E2F8 is absent in differentiating cells, whereas E2F3A transiently peaks in cells exiting the cell cycle prior to terminally differentiating, and canonical repressor E2F4 permanently accumulates in the nucleus of differentiating and differentiated cells. Together, these observations expose an E2F expression landscape that is highly coordinated with respect to cell proliferation and differentiation.

Nuclear Accumulation of E2F3A, E2F4, and E2F8 Is Temporally Phased

To determine the temporal expression of E2Fs relative to each other, we used dual immunofluorescence and developed deep learning tools that allow the systematic, unbiased, and reproducible quantification of multiple E2F proteins in complex proliferating tissues (Figures S6A and S6B). Application of these methods to the intestinal epithelium of E13.5 embryos showed a significant number of E2F3A- and E2F8-negative, single- and double-positive cells in *E2f8*$^{myc/myc}$ stained sections as well as E2F3A- and E2F4-negative, single- and double-positive cells in *E2f4*$^{myc/myc}$ stained sections (Figures 4A, 4B, 4D, and 4E; Table S2). Normalized E2F3A, E2F8, and E2F4 fluorescent intensities were then arbitrarily divided into quartiles and plotted as intensity histograms (Figures 4C and 4F; Table S3). This analysis showed that the nuclear accumulation of E2F3A and E2F8 was partly overlapping, whereas the accumulation of E2F3A and E2F4 was more distantly phased relative to each other.

The ventricular zone of *E2f8*$^{myc/myc}$ embryonic brain sections contained E2F3A- and E2F8-negative, single-positive cells as

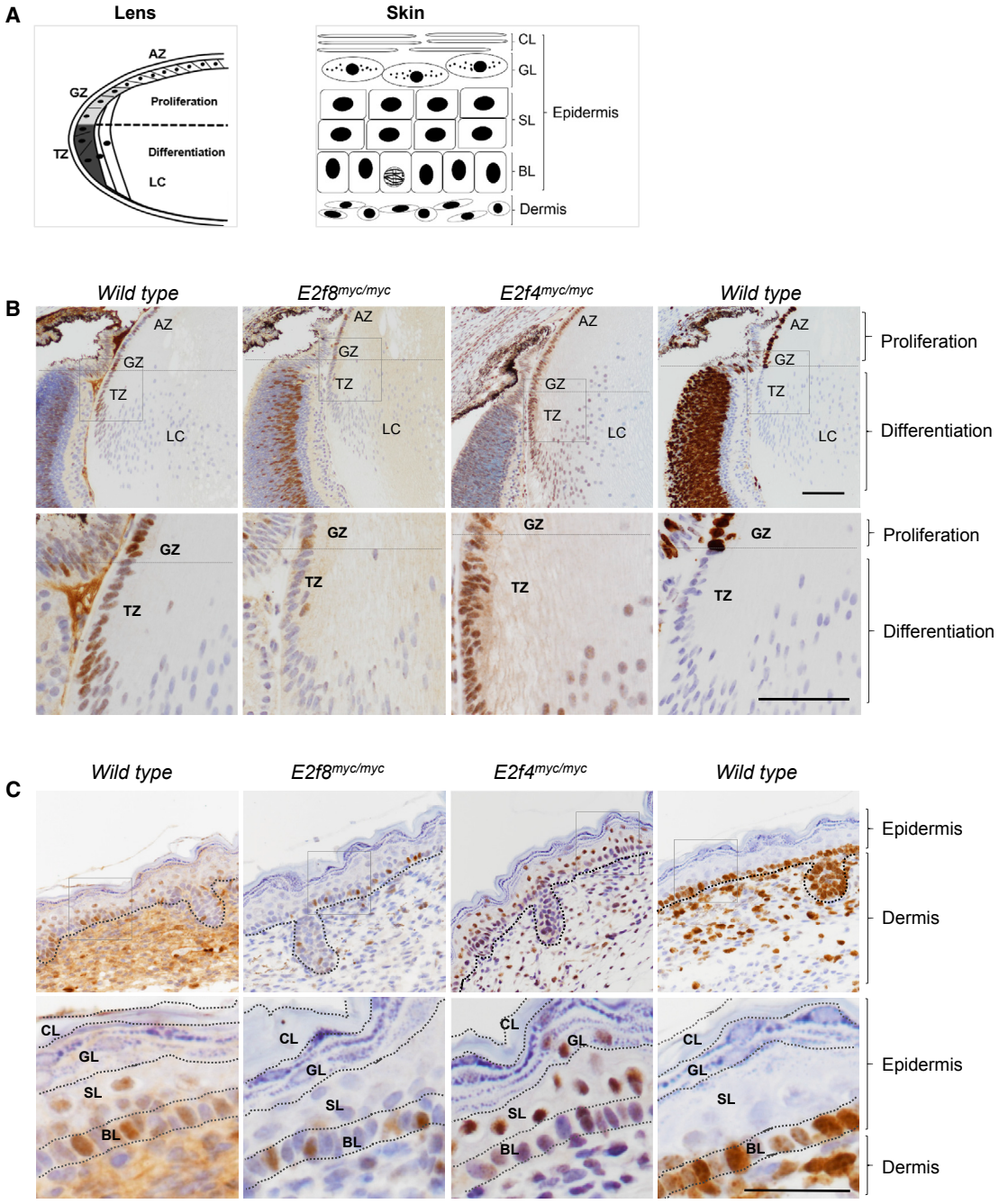

Figure 3. Expression of E2F3A, E2F8, and E2F4 in the Lens and Epidermis

(A) Left: diagram of lens architecture. AZ, anterior zone; GZ, germinative zone; TZ, transition zone; LC, lens cortex. Right: scheme of the neonatal mouse skin epidermal layers. BL, basal layer; SL, spinous layer; GL, granular layer; CL, cornified layer. Proliferation is restricted to the basal layer.

(B) E2F3A, E2F8, E2F4, and Ki67 IHC (left to right) on the neonatal lens of mice with indicated genotypes. The estimated position of the lens equator is marked by a dashed line.

(C) E2F3A, E2F8, E2F4, and Ki67 IHC (left to right) on the neonatal epidermis of mice with indicated genotypes.

E2F8 and E2F4 were detected using MYC antibody. In (B) and (C), higher magnification of the boxed area is shown in the bottom panels. Tissues were counterstained with hematoxylin. Scale bars represent 200 μm (B) and 100 μm (C).

well as an abundance of double-positive cells displaying a spectrum of orange-yellow fluorescent nuclei that reflected their relative amounts (Figure 5A). In contrast, the analysis of *E2f4*$^{myc/myc}$ embryonic brains revealed nuclei that were mainly red or green, with few strongly double-stained E2F3A and E2F4 nuclei (Figure 5B). These patterns of E2F3A-8 and E2F3A-4 expression

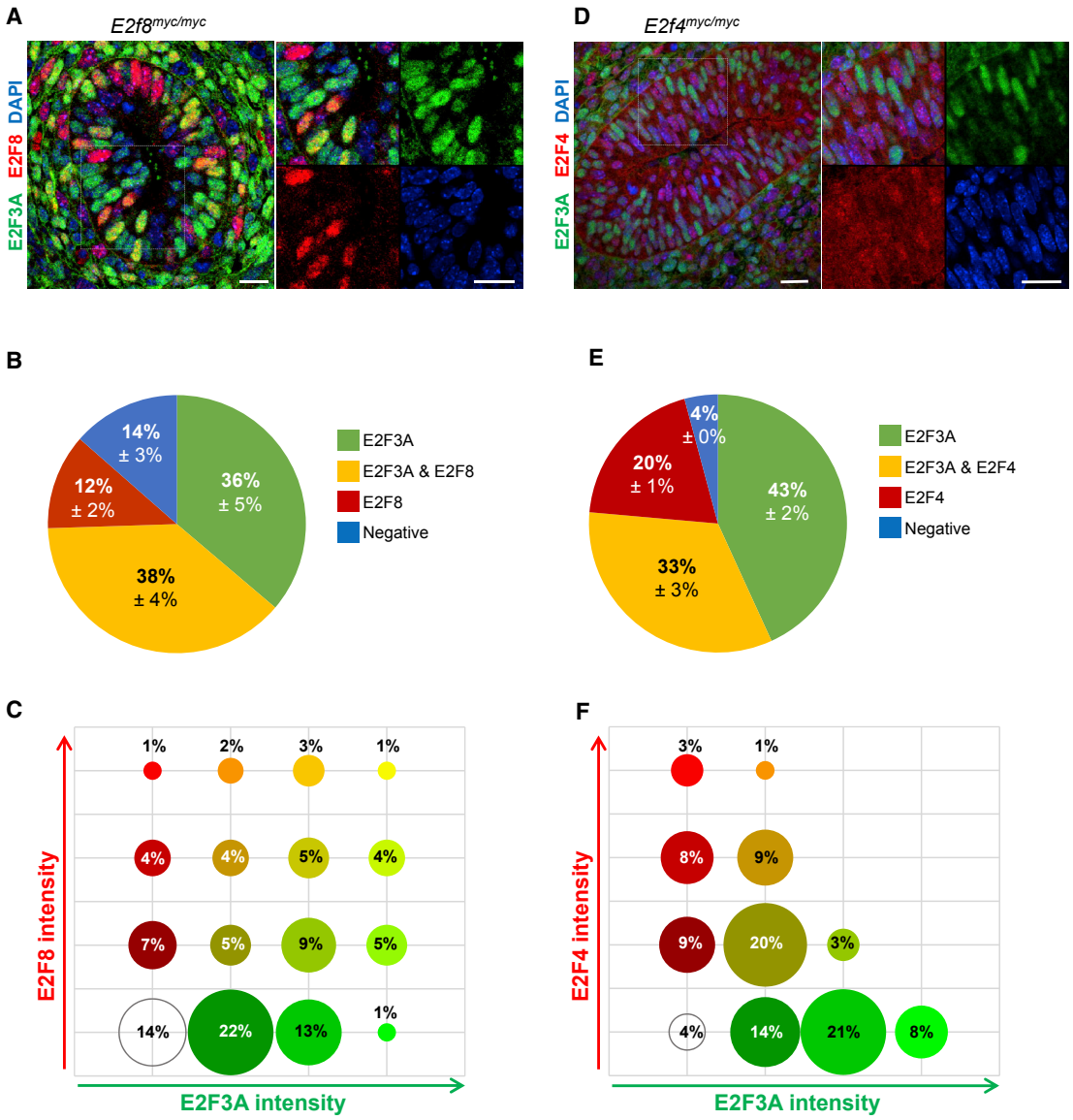

Figure 4. Sequential Expression of E2F3A, E2F4, and E2F8 in Cycling Cells

(A) E2F3A (green) and E2F8 (red) immunofluorescence on the intestine of E13.5 *E2f8*$^{myc/myc}$ embryos. E2F8 was detected using MYC antibody (DAPI counterstain [blue]).

(B) Automated quantification of the staining shown in (A). Data are presented as mean ± SD; n = 3 mice.

(C) 2D histograms depicting the distribution of E2F3A and E2F8's normalized nuclear intensity. Circle size is proportional to the percentage of nuclei.

(D) E2F3A (green) and E2F4 (red) immunofluorescence on the intestine of E13.5 *E2f4*$^{myc/myc}$ embryos. E2F4 was detected using MYC antibody (DAPI counterstain [blue]).

(E) Automated quantification of the staining shown in (D). Data are presented as mean ± SD; n = 2 mice.

(F) 2D histograms depicting the distribution of E2F3A and E2F4's normalized nuclear intensity. Circle size is proportional to the percentage of nuclei.

Images in (A) and (D) are confocal micrographs. Composite and color-split images of the boxed area are shown in the right panels; top left, composite; top right, green channel; bottom left, red channel; bottom right, blue channel. Scale bars, 20 μm. See also Figure S6 and Tables S2 and S3.

were remarkably similar across all other embryonic and adult tissues examined (Figures S6C–S6F). Together, the evaluation of proliferating tissues at the single-cell level suggested that nuclear accumulation of E2F3A, E2F8, and E2F4 is temporally phased, and while partially overlapping, their peak accumulation is temporally distinct.

Peak Expression of E2F3A in G_1-S, E2F8 in S, and E2F4 in Both G_1 and S-G_2

A key feature of E2F3A, E2F4, and E2F8 nuclear accumulation in proliferating tissues is the remarkable periodicity, suggesting an E2F expression landscape that is cell-cycle regulated. To determine the timing of E2F3A, E2F4, and E2F8 expression relative to

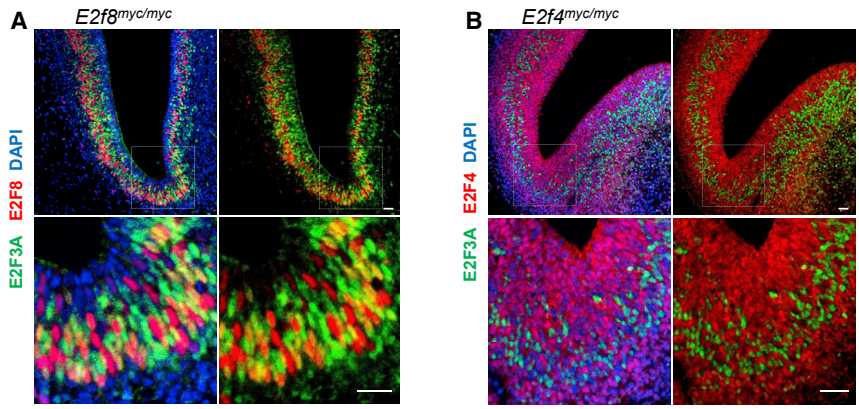

Figure 5. Distinct Temporal Expression of E2F3A, E2F4, and E2F8

(A) E2F3A (green) and E2F8 (red) immunofluorescence on the brain (ventricular zone) of *E2f8*$^{myc/myc}$ E13.5 embryos. E2F8 was detected using MYC antibody (DAPI counterstain [blue]).

(B) E2F3A (green) and E2F4 (red) immunofluorescence on the brain (ventricular zone) of *E2f4*$^{myc/myc}$ E13.5 embryos. E2F4 was detected using MYC antibody (DAPI counterstain [blue]).

In (A) and (B), higher magnification of the boxed area is shown in the bottom panels. Color-split images (green and red channels only) are shown in the right panels. Scale bars, 20 μm. See also Figure S6.

specific cell-cycle phases, we evaluated the accumulation of each E2F family member in conjunction with two cell-cycle markers that identify discrete events in S, G_2, and M phases: 5-ethynyl-2′-deoxyuridine (EdU) incorporation into DNA and histone H3 S10 phosphorylation (pH3). Examination of developing wild-type tissues for EdU incorporation and pH3 immunostaining confirmed their predicted cell-cycle-dependent patterns. Two patterns of EdU fluorescent staining distinguished early from late S phase: diffuse nuclear staining (EdU-Di) in early to mid S phase and variably sized spots juxtaposed to the nuclear membrane (EdU-Pu) in mid-late S phase (Figure 6A) (O'Keefe et al., 1992; Yamada et al., 2005). Two patterns of pH3 immunostaining distinguished S-G_2 and mitosis (Figure 6A); fluorescent puncta in late S and in G_2 (pH3-Pu), and diffuse nuclear staining in mitotic cells (pH3-Di) (Barber et al., 2004). Integrating the staining patterns for these two markers allow events between S phase and mitosis to be placed in a precise sequence as illustrated in Figure 6B.

Immunostaining of wild-type embryos with E2F3A and either EdU or pH3 revealed a partial overlap between E2F3A expression and EdU-Di, EdU-Pu, and pH3-Pu labeling (Figure 6C). Quantification of fluorescent images using our developed deep learning methods showed that 75% of intestinal epithelial cells had some detectable level of E2F3A expression, with a half of the E2F3A-positive cells being negative for EdU (Figure 6D; Table S2). All EdU-Di-positive cells and most, but not all, EdU-Pu-positive cells were stained for E2F3A. These assays indicated that E2F3A expression does not extend into late S phase but instead is limited to early-mid S phase. The large number of singly stained E2F3A-positive cells is thus presumed to be in G_1. Consistent with this interpretation, double staining with E2F3A and pH3 showed that one-third of E2F3A-positive cells were pH3-Pu positive but none were pH3-Di positive (Figures 6C and 6D; Table S2). These findings suggested that E2F3A expression spans G_1 to mid S phase. Immunostaining of additional wild-type embryonic and adult tissues with either EdU or pH3 confirmed a similar cell-cycle pattern of E2F3A expression (Figures S7A–S7C).

Immunostaining of *E2f8*$^{myc/myc}$ embryos for E2F8 and either EdU or pH3 revealed a prominent overlap between E2F8 expression and EdU-Di, EdU-Pu, and pH3-Pu labeling (Figure 6E). Quantification of the fluorescent staining in the intestinal epithelium showed that 50% of cells expressed some level of E2F8 (Figure 6F; Table S2). Approximately 20% of E2F8 positive cells were negative for EdU, whereas essentially all EdU-Di- and EdU-Pu-positive cells were E2F8 positive. Double staining for E2F8 and pH3 showed the vast majority of pH3-Pu-positive cells but none of pH3-Di-positive cells expressed E2F8 (Figures 6E and 6F; Table S2). These observations suggested that E2F8 expression starts in S phase and disappears in late G_2 or early M phase (Figure 6F). Immunostaining of additional *E2f8*$^{myc/myc}$ embryonic and adult tissues with either EdU or pH3 confirmed a similar cell cycle pattern of E2F8 expression (Figures S7D–S7F). FOXM1 protein stability is tightly cell-cycle regulated, accumulating from mid S phase to mitosis (Laoukili et al., 2005), and was thus used as an additional cell-cycle-specific marker to validate E2F3A's G_1-S-specific expression and E2F8's S-G_2-specific expression (Figure S7G–S7J).

Quantification of dual-fluorescent staining of *E2f4*$^{myc/myc}$ embryos with E2F4 and either EdU or pH3 showed that approximately half of the cells in the intestinal epithelium exhibited some level of nuclear E2F4 expression and were mostly singly stained (Figures 6G and 6H; Table S2). All EdU-Di and pH3-Di cells were negative for nuclear E2F4, and close to a half of either EdU-Pu or pH3-Pu cells expressed nuclear E2F4. These analyses revealed that nuclear E2F4 accumulates in a biphasic pattern that includes a period in G_1 and another period in late S-G_2 (Figure 6H; Table S2). Immunostaining of additional *E2f4*$^{myc/myc}$ embryonic and adult tissues with either EdU or pH3 confirmed a similar cell-cycle pattern of E2F4 expression (Figures S7K–S7M).

Lastly, we estimated the temporal evolution of E2F3A, E2F8, and E2F4's nuclear accumulation in relationship to the cell cycle (Figures 4, 6, S5G, and S5H). With the assumption that expression levels (fluorescent intensities) follow a concave parabolic pattern and that time is proportional to the number of cells observed, the temporal dynamics of E2F3A, E2F8, and E2F4 in the cell cycle were estimated (Figure 7A). This analysis suggested that E2F3A, E2F8, and E2F4 are sequentially expressed in proliferating cells, with E2F3A peaking in G_1-S, E2F8 in mid to late S, and E2F4 peaking in both G_1 and G_2 (Figure 7B). Together, our findings provide a remarkably uniform

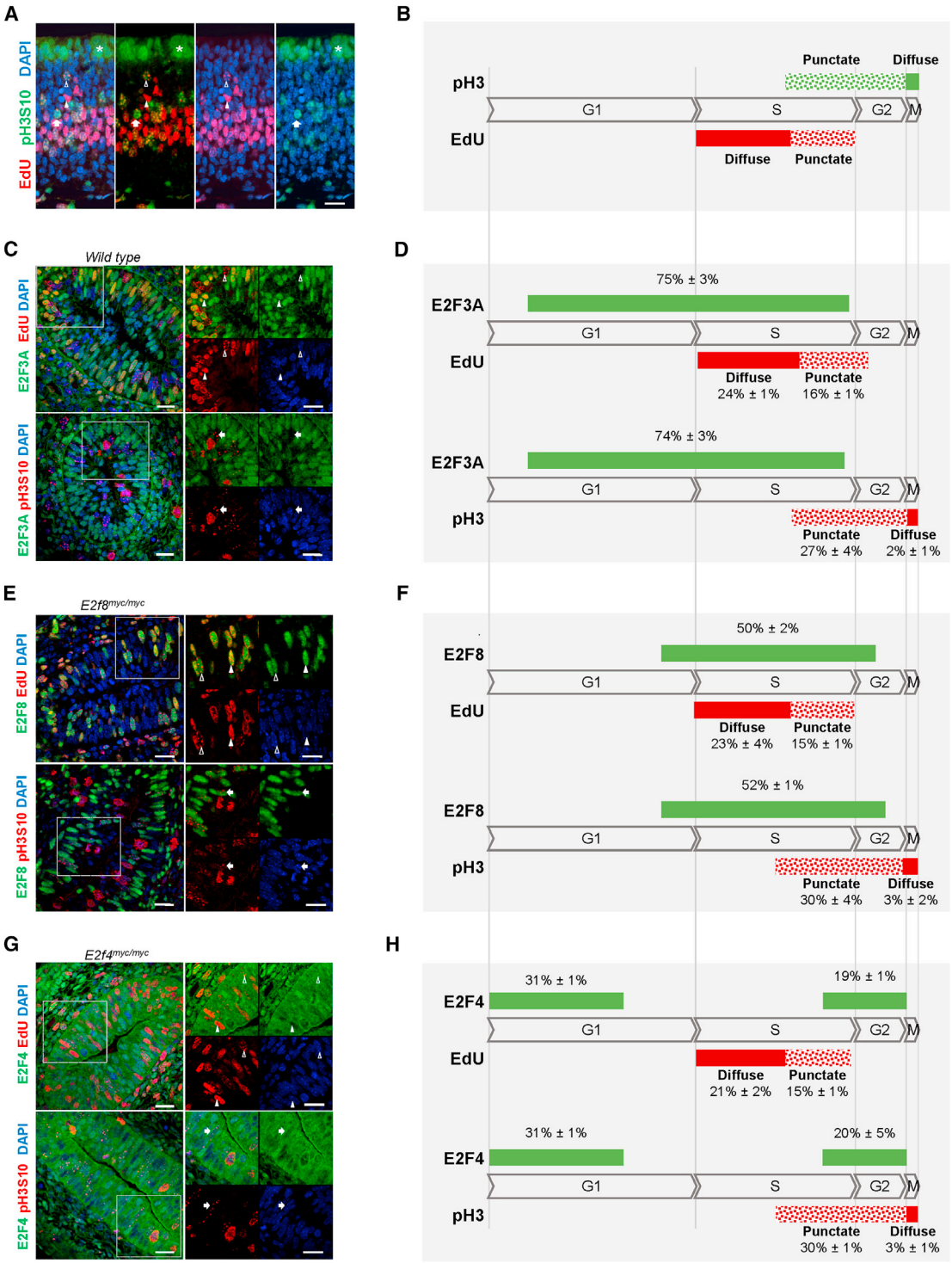

Figure 6. Peak Expression of E2F3A in G_1-S, E2F8 in S, and E2F4 in G_1 and S-G_2

(A) Immunofluorescence of EdU (red) and pH3 (green) in the ventricular zone of the brain of E13.5 wild-type embryos (DAPI counterstain [blue]). Left, composite image; middle left, green and red channels; middle right, red and blue channels; right, green and blue channels.

(B) Schematic of the proposed distinct temporal patterns of EdU and pH3 displayed in (A).

(C) Immunofluorescence of EdU (red) and E2F3A (green) (top), and pH3 (red) and E2F3A (green) (bottom), on the intestine of E13.5 wild-type embryos (DAPI counterstain [blue]).

(legend continued on next page)

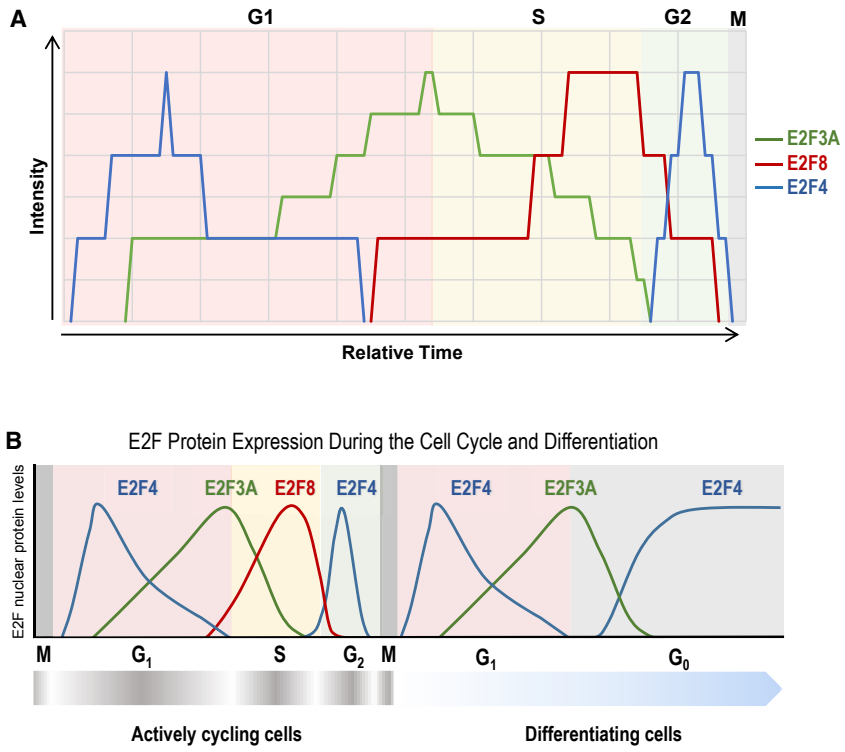

Figure 7. Integrative Analysis of Cell-Cycle-Dependent Nuclear Accumulation of E2Fs

(A) Estimated temporal dynamics of E2F3A, E2F8, and E2F4 expression (see STAR Methods for details).

(B) Diagram of the proposed cell-cycle-dependent expression of E2Fs.

spatiotemporal landscape of how E2F activators and repressors sequentially accumulate in living organisms to support orchestrated waves of activation and repression that underlie cell-cycle-dependent oscillations in gene expression.

DISCUSSION

Orchestrating cell-cycle-dependent mRNA oscillations is critical to cell proliferation and development in multicellular organisms. Unbiased transcriptomic profiling of G_0, G_1-S, and S-G_2-M sorted cells from mouse embryos suggested a central role for E2Fs in the control of cell-cycle-dependent gene expression. The CDK-RB-E2F pathway is believed to coordinate cell proliferation and differentiation by regulating cell-cycle-dependent gene expression programs (Bertoli et al., 2013; Malumbres and Barbacid, 2009). A large body of research in a variety of organisms and mammalian cell lines suggests that oscillations in cell-cycle-regulated gene expression result, at least in part, from sequential waves of E2F-mediated transcriptional activation and repression (Giangrande et al., 2004; Li et al., 2008). However, the variety of specialized cell types in mammalian tissues and the complexity of the E2F family have made understanding how E2F activities are coordinated *in vivo* a real challenge. Using tagged-E2F knockin mice, imaging, and deep-learning tools, we mapped the spatial and temporal expression of E2F activators, canonical repressors, and atypical repressors during embryonic and adult development. This identified two exquisitely regulated E2F transcriptional modules, one composed of E2F3A-8-4 and a second composed of E2F3A-4. Based on the analysis of a broad set of tissues during embryonic and adult development of mice, we propose that two distinct E2F modules coordinate mitotic cell-cycle-dependent gene expression in proliferating and differentiating mammalian cells.

E2F or E2F-like proteins regulate cell-cycle-dependent transcription in all eukaryotic organisms, from yeast to mammals. While some functions are shared among E2F family members, other functions are unique and critical for development and a cancer-free lifespan (Attwooll et al., 2004; DeGregori and Johnson, 2006; Kent et al., 2017; Tsai et al., 2008). Consistent with E2Fs having specific physiological functions, genetic and imaging tools described here reveal that activator and repressor E2Fs accumulate and disappear at different phases of the cell cycle (Figure 7B). We show E2F3A levels peak in G_1-S, E2F8 levels peak in mid-late S phase, and nuclear E2F4 levels peak at two distinct phases of the cell cycle, in G_1 and S-G_2. This pattern of E2F regulation is apparent in cells of all organs and at all developmental stages analyzed. These findings are in basic agreement

(D) Automated quantification of E2F3A and EdU (top) and E2F3A and pH3 (bottom) in the intestinal epithelium of E13.5 wild-type embryos. Data are presented as mean ± SD; n = 3 mice.

(E) Immunofluorescence of EdU (red) and E2F8 (green) (top), and pH3 (red) and E2F8 (green) (bottom), on the intestine of *E2f8*$^{myc/myc}$ E13.5 embryos. E2F8 was detected using MYC antibody (DAPI counterstain [blue]).

(F) Automated quantification of E2F8 and EdU (top), and E2F8 and pH3 (bottom) in the intestinal epithelium of *E2f8*$^{myc/myc}$ E13.5 embryos. Data are presented as mean ± SD; n = 3 mice.

(G) Immunofluorescence of EdU (red) and E2F4 (green) (top), and pH3 (red) and E2F4 (green) (bottom) on the intestine of *E2f4*$^{myc/myc}$ E13.5 embryos. E2F4 was detected using MYC antibody (DAPI counterstain [blue]).

(H) Automated quantification of E2F4 and EdU (top) and E2F4 and pH3 (bottom) in the intestinal epithelium of *E2f4*$^{myc/myc}$ E13.5 embryos. Data are presented as mean ± SD; n = 2 mice.

Images in (C), (E), and (G) are confocal micrographs. Composite and color-split images of the boxed area are shown on right panels; top left, green and red channels; top right, green channel; bottom left, red channel; bottom right, blue channel. Solid arrowhead, EdU diffuse (EdU-Di); open arrowhead, EdU punctate (EdU-Pu); arrow, pH3 punctate (pH3-Pu); asterisk, pH3 diffuse (pH3-Di). Scale bars, 20 μm. See also Figure S7 and Table S2.

with the existing model of E2F function derived from the bulk analysis of mRNA, protein, and DNA-binding activity in selected cell lines grown *in vitro*. The present single-cell-level *in vivo* analysis suggests that E2F protein levels oscillate in proliferating cells of all mitotic mouse tissues analyzed, including tissue specific progenitors of embryonic and adult organs, establishing a refined, universal, and physiologically relevant model of how E2Fs are expressed and, presumably, function in mammals.

Besides transcriptional mechanisms, post-transcriptional regulation is known to play an important role in the temporal control of E2F-dependent transcription. Ubiquitin-mediated protein degradation has been proposed to regulate the activity of several E2Fs *in vitro* (Boekhout et al., 2016; Marti et al., 1999; Ping et al., 2012). Whereas mRNA levels of E2F activators and atypical repressors increased similarly as cells moved from G_0 to G_1, S-G_2, and M, peak protein levels of E2F3A and E2F8 were clearly temporally distinct during the cell cycle, with only a partial overlap during S phase. This might indicate that transcriptional regulation of these E2F family members is only important for their accumulation but that targeted protein degradation may be required to confine their protein accumulation to specific phases of the cell cycle (Clijsters et al., 2019). A major mechanism regarding the functional regulation of E2F4 involves nuclear-cytoplasmic shuttling (Gaubatz et al., 2000; 2001; Leone et al., 1998; Lindeman et al., 1997; Puri et al., 1998). Our analysis revealed that even though E2F4 is mostly cytoplasmic in cycling cells, the protein transiently accumulates in the nucleus twice during the cell cycle, first in early G_1 and then again in S-G_2. Overall, our observations show that cell-cycle-dependent gene expression is under constant control by either E2F repressors or activators. We suggest that the sequential nuclear accumulation and disappearance of E2F3A, E2F8, and E2F4 form an E2F module used to drive waves of activation and repression that support cell-cycle-dependent oscillations in gene expression necessary for cell divisions.

Our results also identified a second E2F module composed of E2F3A and E2F4 used to extinguish cell-cycle-dependent gene expression in cells programmed to exit the cell cycle and differentiate (Figure 7B). Analysis of the lens, epidermis, and other stratified epithelia revealed that as cells transit through mitosis and reenter G_1 for the last time before exiting the cell cycle, E2F3A protein temporarily accumulates prior to permanently disappearing. Thus, in differentiating cells, E2F3A transiently accumulates before prolonged E2F4 accumulation and terminal differentiation. This is interesting because based on *in vitro* work, it was always assumed that the accumulation of activating E2Fs (such as E2F3A) following mitosis would lead to a new cell cycle while those mitotic cells destined to exit the cell cycle would only accumulate E2F4. The *in vivo* data here suggest that cells differentiate not by exiting the cell cycle with accumulation of E2F4 after mitosis but more likely in late G1, with accumulation of activating E2Fs, allowing the choice between entering (initiating DNA replication) or exiting (differentiating) the cell cycle.

At least in the small intestine of mice, the accumulation of E2F3A in the last G_1 coincides with the physical association of hypo-phosphorylated RB (Burkhart and Sage, 2008; Lees et al., 1993; Morris and Dyson, 2001). The subsequent disappearance of E2F3A protein at the crypt-villus junctional zone is tightly coordinated with the nuclear appearance and maintenance of the canonical E2F4 repressor along the entire villus, permanent repression of cell-cycle-regulated genes, and terminal differentiation of enterocytes. Indeed, previous genetic experiments showed that genetic ablation of E2F3A in the small intestine results in derepression of E2F target genes in enterocytes exiting the cell cycle (Chong et al., 2009; Liu et al., 2015) and, importantly, elevated target gene expression is maintained throughout the length of the villus, even though E2F3A is not normally expressed beyond the crypt-villus junctional zone. Together with the restricted transient expression of E2F3A along the proliferation-differentiation axis of the small intestine described here, these observations are consistent with E2F3A and RB forming a transcriptionally repressive complex that is necessary for extinguishing cell-cycle-dependent gene expression during the last G_1 before cells exit the cell cycle and establishing an E2F4-mediated repressive state as enterocytes fully differentiate and migrate into the villus (Chong et al., 2009; Liu et al., 2015).

Why might transcriptional repression in cells actively cycling versus those exiting the cell cycle require two different flavors of E2F repressors? We propose that transcriptional repression relayed by the E2F8-E2F4 axis in mid S-G_2 of cycling cells imposes a temporary repressive state that permits the next wave of cell-cycle-dependent gene expression to be reactivated during the next cell cycle. Transcriptional repression relayed by the E2F3A-E2F4 axis during the last G_1 prior to exiting the cell cycle would instead impose a permanent repressive state that facilitates terminal differentiation programs to be effectively executed and, in the case of epithelial cells, the integrity of cell barriers to be maintained. Presumably, E2F8 in late S phase of cycling cells and E2F3A in the last G_1 prior to exiting the cell cycle are used to recruit different chromatin remodeling machinery that impart distinct histone modifications, setting up different chromatin platforms for E2F4-mediated repression to act on. Indeed, E2F8 lacks the ability to form a repressive complex with RB (Christensen et al., 2005; Maiti et al., 2005) and, presumably, other RB associated proteins. Thus, E2F8 and E2F3A may be viewed to differentially prime chromatin for the subsequent repressive actions of E2F4, and thus support additional cell divisions in the case of E2F8-4 or support quiescence in the case of E2F3A-4. The specific chromatin modifications resulting from the accumulation and recruitment of these two E2F repressive modules (E2F8-4 and E2F3A-4) to target genes have yet to be elucidated. Regardless of the biochemical details, our results identify the critical modular arrangement of E2Fs and the spatial and temporal context in which the two E2F modules are used to coordinate cell-cycle-dependent gene expression during mammalian development.

STAR★METHODS

Detailed methods are provided in the online version of this paper and include the following:

- KEY RESOURCES TABLE
- CONTACT FOR REAGENT AND RESOURCE SHARING
- EXPERIMENTAL MODEL AND SUBJECT DETAILS
  - Mouse models and care
  - Cell culture

Please cite this article in press as: Cuitiño et al., Two Distinct E2F Transcriptional Modules Drive Cell Cycles and Differentiation, Cell Reports (2019), https://doi.org/10.1016/j.celrep.2019.05.004

SUPPLEMENTAL INFORMATION

Supplemental Information can be found online at https://doi.org/10.1016/j.celrep.2019.05.004.

ACKNOWLEDGMENTS

We thank J. Bice and D. Bryant for assistance with histology and M. Parish for assistance with immunohistochemistry. We are grateful to D. Guttridge and L. Kent for reading and critically commenting on the manuscript. We also thank Alina Murphy for assistance with preparation of single-cell suspensions and real-time qPCR. This work was supported by the OSUCCC Genetically Engineered Mouse Modeling, Genomics, Analytical Cytometry Core Shared Resources and the Campus Microscopy and Imaging Facility at The Ohio State University and supported in part by grant P30 CA016058, by the HCC Cellular Microscopy Imaging Facility at the Medical University of South Carolina, and by grant P30 CA138313, National Cancer Institute, Bethesda, MD. The Titan Xp used for this research was donated by the NVIDIA Corporation. This work was funded by an NIH grant to G.L. (R01CA121275) and by a Chan Zuckerberg Initiative DAF grant to T.P. (2019-198009).

AUTHOR CONTRIBUTIONS

M.C.C. and G.L. designed the experiments. M.C.C. and D.S. bred, genotyped, and harvested mice. M.C.C. and A.P.C. prepared single-cell suspensions and optimized the FACS protocol. M.C.C. and N. Shinde performed real-time qPCR. T.L. performed RNA isolations and library preparation for RNA-seq. D.S. and A.W. preprocessed the RNA-seq data, with supervision from C.T. T.P. performed the bioinformatic analysis of RNA-seq data. D.S. generated the targeting vectors, and V.C. generated the knockin mice. R.K. developed immunofluorescence and immunohistochemistry protocols. M.C.C. performed wide-field and confocal microscopy imaging and qualitative and quantitative manual analysis of immunostaining. T.P. designed and performed automated quantification of immunostaining. R.S. assisted with mouse genotyping and manual quantification of immunostaining. T.O.-U. and S.I.B. performed western blots. G.L. supervised the studies. All authors assisted with data interpretation and manuscript review. M.C.C., T.P., and D.S. prepared figures. M.C.C., M.C.O., and G.L. wrote the manuscript with input from all authors.

DECLARATION OF INTERESTS

The authors declare no competing interests.

Received: October 31, 2018
Revised: April 14, 2019
Accepted: April 30, 2019
Published: May 23, 2019

REFERENCES

Adams, M.R., Sears, R., Nuckolls, F., Leone, G., and Nevins, J.R. (2000). Complex transcriptional regulatory mechanisms control expression of the E2F3 locus. Mol. Cell. Biol. *20*, 3633–3639.

Anders, S., Pyl, P.T., and Huber, W. (2015). HTSeq—a Python framework to work with high-throughput sequencing data. Bioinformatics *31*, 166–169.

Attwooll, C., Lazzerini Denchi, E., and Helin, K. (2004). The E2F family: specific functions and overlapping interests. EMBO J. *23*, 4709–4716.

Barber, C.M., Turner, F.B., Wang, Y., Hagstrom, K., Taverna, S.D., Mollah, S., Ueberheide, B., Meyer, B.J., Hunt, D.F., Cheung, P., and Allis, C.D. (2004). The enhancement of histone H4 and H2A serine 1 phosphorylation during mitosis and S-phase is evolutionarily conserved. Chromosoma *112*, 360–371.

Barker, N., van Es, J.H., Kuipers, J., Kujala, P., van den Born, M., Cozijnsen, M., Haegebarth, A., Korving, J., Begthel, H., Peters, P.J., and Clevers, H. (2007). Identification of stem cells in small intestine and colon by marker gene Lgr5. Nature *449*, 1003–1007.

Bertoli, C., Skotheim, J.M., and de Bruin, R.A. (2013). Control of cell cycle transcription during G1 and S phases. Nat. Rev. Mol. Cell Biol. *14*, 518–528.

Blanpain, C., and Fuchs, E. (2006). Epidermal stem cells of the skin. Annu. Rev. Cell Dev. Biol. *22*, 339–373.

Boekhout, M., Yuan, R., Wondergem, A.P., Segeren, H.A., van Liere, E.A., Awol, N., Jansen, I., Wolthuis, R.M., de Bruin, A., and Westendorp, B. (2016). Feedback regulation between atypical E2Fs and APC/CCdh1 coordinates cell cycle progression. EMBO Rep. *17*, 414–427.

Burkhart, D.L., and Sage, J. (2008). Cellular mechanisms of tumour suppression by the retinoblastoma gene. Nat. Rev. Cancer *8*, 671–682.

Byrne, C., and Hardman, M. (2002). Integumentary structures. In Mouse Development Patterning Morphogenesis and Organogenesis, R. Janet and P.T. Tam, eds. (Academic Press).

Campton, D.E., Ramirez, A.B., Nordberg, J.J., Drovetto, N., Clein, A.C., Varshavskaya, P., Friemel, B.H., Quarre, S., Breman, A., Dorschner, M., et al. (2015). High-recovery visual identification and single-cell retrieval of circulating tumor cells for genomic analysis using a dual-technology platform integrated with automated immunofluorescence staining. BMC Cancer *15*, 360.

Chen, H.-Z., Tsai, S.-Y., and Leone, G. (2009). Emerging roles of E2Fs in cancer: an exit from cell cycle control. Nat. Rev. Cancer *9*, 785–797.

Chong, J.-L., Wenzel, P.L., Sáenz-Robles, M.T., Nair, V., Ferrey, A., Hagan, J.P., Gomez, Y.M., Sharma, N., Chen, H.-Z., Ouseph, M., et al. (2009). E2f1-3 switch from activators in progenitor cells to repressors in differentiating cells. Nature *462*, 930–934.

Christensen, J., Cloos, P., Toftegaard, U., Klinkenberg, D., Bracken, A.P., Trinh, E., Heeran, M., Di Stefano, L., and Helin, K. (2005). Characterization of E2F8, a novel E2F-like cell-cycle regulated repressor of E2F-activated transcription. Nucleic Acids Res. *33*, 5458–5470.

Clijsters, L., Hoencamp, C., Calis, J., Marzio, A., Handgraaf, S., Cuitino, M., Marzluff, W., Rosenberg, B., Leobe, G., and Pagano, M. (2019). Cyclin F controls cell cycle transcriptional outputs by directing the degradation of the three activator E2Fs. Mol Cell *74*, Published online May 23, 2019. https://doi.org/10.1016/j.molcel.2019.04.010.

Cordon-Cardo, C. (1995). Mutations of cell cycle regulators. Biological and clinical implications for human neoplasia. Am. J. Pathol. *147*, 545–560.

Cross, F.R., Buchler, N.E., and Skotheim, J.M. (2011). Evolution of networks and sequences in eukaryotic cell cycle control. Philos. Trans. R. Soc. Lond. B Biol. Sci. *366*, 3532–3544.

Danielian, P.S., Friesenhahn, L.B., Faust, A.M., West, J.C., Caron, A.M., Bronson, R.T., and Lees, J.A. (2008). E2f3a and E2f3b make overlapping but different contributions to total E2f3 activity. Oncogene *27*, 6561–6570.

DeGregori, J., and Johnson, D.G. (2006). Distinct and overlapping roles for E2F family members in transcription, proliferation and apoptosis. Curr. Mol. Med. *6*, 739–748.

Di Stefano, L., Jensen, M.R., and Helin, K. (2003). E2F7, a novel E2F featuring DP-independent repression of a subset of E2F-regulated genes. EMBO J. *22*, 6289–6298.

Dobin, A., Davis, C.A., Schlesinger, F., Drenkow, J., Zaleski, C., Jha, S., Batut, P., Chaisson, M., and Gingeras, T.R. (2013). STAR: ultrafast universal RNA-seq aligner. Bioinformatics *29*, 15–21.

Field, S.J., Tsai, F.-Y., Kuo, F., Zubiaga, A.M., Kaelin, W.G., Jr., Livingston, D.M., Orkin, S.H., and Greenberg, M.E. (1996). E2F-1 functions in mice to promote apoptosis and suppress proliferation. Cell *85*, 549–561.

Gaubatz, S., Lindeman, G.J., Ishida, S., Jakoi, L., Nevins, J.R., Livingston, D.M., and Rempel, R.E. (2000). E2F4 and E2F5 play an essential role in pocket protein-mediated G1 control. Mol. Cell *6*, 729–735.

Gaubatz, S., Lees, J.A., Lindeman, G.J., and Livingston, D.M. (2001). E2F4 is exported from the nucleus in a CRM1-dependent manner. Mol. Cell. Biol. *21*, 1384–1392.

Giangrande, P.H., Zhu, W., Schlisio, S., Sun, X., Mori, S., Gaubatz, S., and Nevins, J.R. (2004). A role for E2F6 in distinguishing G1/S- and G2/M-specific transcription. Genes Dev. *18*, 2941–2951.

Ginsberg, D., Vairo, G., Chittenden, T., Xiao, Z.-X., Xu, G., Wydner, K.L., DeCaprio, J.A., Lawrence, J.B., and Livingston, D.M. (1994). E2F-4, a new member of the E2F transcription factor family, interacts with p107. Genes Dev. *8*, 2665–2679.

Glasbey, C.A. (1993). An analysis of histogram-based thresholding algorithms. CVGIP Graph. Models Image Process. *55*, 532–537.

Gotea, V., and Ovcharenko, I. (2008). DiRE: identifying distant regulatory elements of co-expressed genes. Nucleic Acids Res. *36*, W133-9.

Harbour, J.W., and Dean, D.C. (2000). The Rb/E2F pathway: expanding roles and emerging paradigms. Genes Dev. *14*, 2393–2409.

Hayashi, S., Lewis, P., Pevny, L., and Mcmahon, A.P. (2002). Efficient gene modulation in mouse epiblast using a Sox2Cre transgenic mouse strain. Gene Expr. Patterns. *2*, 93–97.

Henley, S.A., and Dick, F.A. (2012). The retinoblastoma family of proteins and their regulatory functions in the mammalian cell division cycle. Cell Div. *7*, 10.

Huang, L.-K., and Wang, M.-J.J. (1995). Image thresholding by minimizing the measures of fuzziness. Pattern Recognit. *28*, 41–51.

Humbert, P.O., Rogers, C., Ganiatsas, S., Landsberg, R.L., Trimarchi, J.M., Dandapani, S., Brugnara, C., Erdman, S., Schrenzel, M., Bronson, R.T., and Lees, J.A. (2000a). E2F4 is essential for normal erythrocyte maturation and neonatal viability. Mol. Cell *6*, 281–291.

Humbert, P.O., Verona, R., Trimarchi, J.M., Rogers, C., Dandapani, S., and Lees, J.A. (2000b). E2f3 is critical for normal cellular proliferation. Genes Dev. *14*, 690–703.

Iaquinta, P.J., and Lees, J.A. (2007). Life and death decisions by the E2F transcription factors. Curr. Opin. Cell Biol. *19*, 649–657.

Kent, L.N., Rakijas, J.B., Pandit, S.K., Westendorp, B., Chen, H.-Z., Huntington, J.T., Tang, X., Bae, S., Srivastava, A., Senapati, S., et al. (2016). E2f8 mediates tumor suppression in postnatal liver development. J. Clin. Invest. *126*, 2955–2969.

Kent, L.N., Bae, S., Tsai, S.-Y., Tang, X., Srivastava, A., Koivisto, C., Martin, C.K., Ridolfi, E., Miller, G.C., Zorko, S.M., et al. (2017). Dosage-dependent copy number gains in E2f1 and E2f3 drive hepatocellular carcinoma. J. Clin. Invest. *127*, 830–842.

Korenjak, M., Taylor-Harding, B., Binné, U.K., Satterlee, J.S., Stevaux, O., Aasland, R., White-Cooper, H., Dyson, N., and Brehm, A. (2004). Native E2F/RBF complexes contain Myb-interacting proteins and repress transcription of developmentally controlled E2F target genes. Cell *119*, 181–193.

Lammens, T., Li, J., Leone, G., and De Veylder, L. (2009). Atypical E2Fs: new players in the E2F transcription factor family. Trends Cell Biol. *19*, 111–118.

Laoukili, J., Kooistra, M.R., Brás, A., Kauw, J., Kerkhoven, R.M., Morrison, A., Clevers, H., and Medema, R.H. (2005). FoxM1 is required for execution of the mitotic programme and chromosome stability. Nat. Cell Biol. *7*, 126–136.

Lees, J.A., Saito, M., Vidal, M., Valentine, M., Look, T., Harlow, E., Dyson, N., and Helin, K. (1993). The retinoblastoma protein binds to a family of E2F transcription factors. Mol. Cell. Biol. *13*, 7813–7825.

Leone, G., DeGregori, J., Yan, Z., Jakoi, L., Ishida, S., Williams, R.S., and Nevins, J.R. (1998). E2F3 activity is regulated during the cell cycle and is required for the induction of S phase. Genes Dev. *12*, 2120–2130.

Leone, G., Nuckolls, F., Ishida, S., Adams, M., Sears, R., Jakoi, L., Miron, A., and Nevins, J.R. (2000). Identification of a novel E2F3 product suggests a mechanism for determining specificity of repression by Rb proteins. Mol. Cell. Biol. *20*, 3626–3632.

Li, C., and Tam, P.K.-S. (1998). An iterative algorithm for minimum cross entropy thresholding. Pattern Recognit. Lett. *19*, 771–776.

Li, J., Ran, C., Li, E., Gordon, F., Comstock, G., Siddiqui, H., Cleghorn, W., Chen, H.-Z., Kornacker, K., Liu, C.-G., et al. (2008). Synergistic function of E2F7 and E2F8 is essential for cell survival and embryonic development. Dev. Cell *14*, 62–75.

Li, H., Handsaker, B., Wysoker, A., Fennell, T., Ruan, J., Homer, N., Marth, G., Abecasis, G., and Durbin, R.; 1000 Genome Project Data Processing Subgroup (2009). The Sequence Alignment/Map format and SAMtools. Bioinformatics *25*, 2078–2079.

Lindeman, G.J., Gaubatz, S., Livingston, D.M., and Ginsberg, D. (1997). The subcellular localization of E2F-4 is cell-cycle dependent. Proc. Natl. Acad. Sci. USA *94*, 5095–5100.

Lindeman, G.J., Dagnino, L., Gaubatz, S., Xu, Y., Bronson, R.T., Warren, H.B., and Livingston, D.M. (1998). A specific, nonproliferative role for E2F-5 in choroid plexus function revealed by gene targeting. Genes Dev. *12*, 1092–1098.

Liu, H., Tang, X., Srivastava, A., Pécot, T., Daniel, P., Hemmelgarn, B., Reyes, S., Fackler, N., Bajwa, A., Kladney, R., et al. (2015). Redeployment of Myc and E2f1-3 drives Rb-deficient cell cycles. Nat. Cell Biol. *17*, 1036–1048.

Logan, N., Graham, A., Zhao, X., Fisher, R., Maiti, B., Leone, G., and La Thangue, N.B. (2005). E2F-8: an E2F family member with a similar organization of DNA-binding domains to E2F-7. Oncogene *24*, 5000–5004.

Love, M.I., Huber, W., and Anders, S. (2014). Moderated estimation of fold change and dispersion for RNA-seq data with DESeq2. Genome Biol. *15*, 550.

Magae, J., Wu, C.L., Illenye, S., Harlow, E., and Heintz, N.H. (1996). Nuclear localization of DP and E2F transcription factors by heterodimeric partners and retinoblastoma protein family members. J. Cell Sci. *109*, 1717–1726.

Maiti, B., Li, J., de Bruin, A., Gordon, F., Timmers, C., Opavsky, R., Patil, K., Tuttle, J., Cleghorn, W., and Leone, G. (2005). Cloning and characterization of mouse E2F8, a novel mammalian E2F family member capable of blocking cellular proliferation. J. Biol. Chem. *280*, 18211–18220.

Malumbres, M., and Barbacid, M. (2009). Cell cycle, CDKs and cancer: a changing paradigm. Nat. Rev. Cancer *9*, 153–166.

Marti, A., Wirbelauer, C., Scheffner, M., and Krek, W. (1999). Interaction between ubiquitin-protein ligase SCFSKP2 and E2F-1 underlies the regulation of E2F-1 degradation. Nat. Cell Biol. *1*, 14–19.

Mochizuki, T., and Masai, I. (2014). The lens equator: a platform for molecular machinery that regulates the switch from cell proliferation to differentiation in the vertebrate lens. Dev. Growth Differ. *56*, 387–401.

Morgenstern, J.P., and Land, H. (1990). Advanced mammalian gene transfer: high titre retroviral vectors with multiple drug selection markers and a complementary helper-free packaging cell line. Nucleic Acids Res. *18*, 3587–3596.

Morris, E.J., and Dyson, N.J. (2001). Retinoblastoma protein partners. Adv. Cancer Res. *82*, 1–54.

Murga, M., Fernández-Capetillo, O., Field, S.J., Moreno, B., Borlado, L.R., Fujiwara, Y., Balomenos, D., Vicario, A., Carrera, A.C., Orkin, S.H., et al. (2001). Mutation of E2F2 in mice causes enhanced T lymphocyte proliferation, leading to the development of autoimmunity. Immunity *15*, 959–970.

Nevins, J.R., Leone, G., DeGregori, J., and Jakoi, L. (1997). Role of the Rb/E2F pathway in cell growth control. J. Cell. Physiol. *173*, 233–236.

Please cite this article in press as: Cuitiño et al., Two Distinct E2F Transcriptional Modules Drive Cell Cycles and Differentiation, Cell Reports (2019), https://doi.org/10.1016/j.celrep.2019.05.004

O'Keefe, R.T., Henderson, S.C., and Spector, D.L. (1992). Dynamic organization of DNA replication in mammalian cell nuclei: spatially and temporally defined replication of chromosome-specific alpha-satellite DNA sequences. J. Cell Biol. *116*, 1095–1110.

Oki, S., Ohta, T., Shioi, G., Hatanaka, H., Ogasawara, O., Okuda, Y., Kawaji, H., Nakaki, R., Sese, J., and Meno, C. (2018). Integrative analysis of transcription factor occupancy at enhancers and disease risk loci in noncoding genomic regions. bioRxiv. https://doi.org/10.1101/262899.

Otto, T., and Sicinski, P. (2017). Cell cycle proteins as promising targets in cancer therapy. Nat. Rev. Cancer *17*, 93–115.

Ping, Z., Lim, R., Bashir, T., Pagano, M., and Guardavaccaro, D. (2012). APC/C (Cdh1) controls the proteasome-mediated degradation of E2F3 during cell cycle exit. Cell Cycle *11*, 1999–2005.

Pitarresi, J.R., Liu, X., Sharma, S.M., Cuitiño, M.C., Kladney, R.D., Mace, T.A., Donohue, S., Nayak, S.G., Qu, C., Lee, J., et al. (2016). Stromal ETS2 regulates chemokine production and immune cell recruitment during acinar-to-ductal metaplasia. Neoplasia *18*, 541–552.

Puri, P.L., Cimino, L., Fulco, M., Zimmerman, C., La Thangue, N.B., Giordano, A., Graessmann, A., and Levrero, M. (1998). Regulation of E2F4 mitogenic activity during terminal differentiation by its heterodimerization partners for nuclear translocation. Cancer Res. *58*, 1325–1331.

Rempel, R.E., Saenz-Robles, M.T., Storms, R., Morham, S., Ishida, S., Engel, A., Jakoi, L., Melhem, M.F., Pipas, J.M., Smith, C., and Nevins, J.R. (2000). Loss of E2F4 activity leads to abnormal development of multiple cellular lineages. Mol. Cell *6*, 293–306.

Rodríguez, C.I., Buchholz, F., Galloway, J., Sequerra, R., Kasper, J., Ayala, R., Stewart, A.F., and Dymecki, S.M. (2000). High-efficiency deleter mice show that FLPe is an alternative to Cre-loxP. Nat. Genet. *25*, 139–140.

Sadasivam, S., and DeCaprio, J.A. (2013). The DREAM complex: master coordinator of cell cycle-dependent gene expression. Nat. Rev. Cancer *13*, 585–595.

Sakaue-Sawano, A., Kurokawa, H., Morimura, T., Hanyu, A., Hama, H., Osawa, H., Kashiwagi, S., Fukami, K., Miyata, T., Miyoshi, H., et al. (2008). Visualizing spatiotemporal dynamics of multicellular cell-cycle progression. Cell *132*, 487–498.

Santos, A., Wernersson, R., and Jensen, L.J. (2015). Cyclebase 3.0: a multi-organism database on cell-cycle regulation and phenotypes. Nucleic Acids Res. *43*, D1140–D1144.

Schindelin, J., Arganda-Carreras, I., Frise, E., Kaynig, V., Longair, M., Pietzsch, T., Preibisch, S., Rueden, C., Saalfeld, S., Schmid, B., et al. (2012). Fiji: an open-source platform for biological-image analysis. Nat. Methods *9*, 676–682.

Schneider, C.A., Rasband, W.S., and Eliceiri, K.W. (2012). NIH Image to ImageJ: 25 years of image analysis. Nat Methods *9*, 671–675.

Sherr, C.J. (1996). Cancer cell cycles. Science *274*, 1672–1677.

Trimarchi, J.M., and Lees, J.A. (2002). Sibling rivalry in the E2F family. Nat. Rev. Mol. Cell Biol. *3*, 11–20.

Tsai, S.-Y., Opavsky, R., Sharma, N., Wu, L., Naidu, S., Nolan, E., Feria-Arias, E., Timmers, C., Opavska, J., de Bruin, A., et al. (2008). Mouse development with a single E2F activator. Nature *454*, 1137–1141.

Van Valen, D.A., Kudo, T., Lane, K.M., Macklin, D.N., Quach, N.T., DeFelice, M.M., Maayan, I., Tanouchi, Y., Ashley, E.A., and Covert, M.W. (2016). Deep learning automates the quantitative analysis of individual cells in live-cell imaging experiments. PLoS Comput. Biol. *12*, e1005177.

Viatour, P., and Sage, J. (2011). Newly identified aspects of tumor suppression by RB. Dis. Model. Mech. *4*, 581–585.

Westendorp, B., Mokry, M., Groot Koerkamp, M.J., Holstege, F.C., Cuppen, E., and de Bruin, A. (2012). E2F7 represses a network of oscillating cell cycle genes to control S-phase progression. Nucleic Acids Res. *40*, 3511–3523.

Wu, L., Timmers, C., Maiti, B., Saavedra, H.I., Sang, L., Chong, G.T., Nuckolls, F., Giangrande, P., Wright, F.A., Field, S.J., and Greenberg, M.E. (2001). The E2F1–3 transcription factors are essential for cellular proliferation. Nature *414*, 457–462.

Xu, J. (2005). Preparation, culture, and immortalization of mouse embryonic fibroblasts. Curr. Protoc. Mol. Biol. *70*, 28.1.1–28.1.8.

Yamada, K., Semba, R., Ding, X., Ma, N., and Nagahama, M. (2005). Discrimination of cell nuclei in early S-phase, mid-to-late S-phase, and G(2)/M-phase by sequential administration of 5-bromo-2′-deoxyuridine and 5-chloro-2′-deoxyuridine. J. Histochem. Cytochem. *53*, 1365–1370.

Zack, G.W., Rogers, W.E., and Latt, S.A. (1977). Automatic measurement of sister chromatid exchange frequency. J. Histochem. Cytochem. *25*, 741–753.

STAR★METHODS

KEY RESOURCES TABLE

REAGENT or RESOURCE	SOURCE	IDENTIFIER
Antibodies		
Rabbit monoclonal anti-Ki67 (clone SP6)	Abcam	Cat# ab16667; RRID: AB_302459
Rabbit polyclonal Anti-pH3-S10	Millipore	Cat# 06-570; RRID: AB_310177
Rabbit polyclonal anti-FoxM1	Santa Cruz	Cat# sc-502; RRID: AB_631523
Mouse monoclonal anti-E2F3a	Millipore	Cat# 05-551; RRID: AB_11211950
Rabbit monoclonal anti-Myc-tag	Cell Signaling Technology	Cat# 2278; RRID: AB_490778
Rabbit polyclonal anti-E2F3	Santa Cruz	Cat# sc-878; RRID: AB_2096807
Mouse monoclonal anti-E2F8	Santa Cruz	Cat# sc-514064
Mouse monoclonal anti-E2F4	Millipore	Cat# MABE160; RRID: AB_10845939
hFAB Rhodamine anti-GAPDH	BIO-RAD	Cat# 12004168
hFAB Rhodamine anti-β-Actin	BIO-RAD	Cat# 12004164
HRP-conjugated anti-rabbit IgG	GE healthcare	Cat# NA934; RRID: AB_772206
HRP-conjugated anti-mouse IgG	Jackson ImmunoResearch Laboratories	Cat# 115-035-174, 115-035-071; RRID: AB_2338512
Chemicals, Peptides, and Recombinant Proteins		
Formalin	ThermoFisher Scientific	Cat# 23-245-685
TRIzol reagent	ThermoFisher Scientific	Cat# 15596018
Protease inhibitor cocktail	Sigma	Cat# P1860
ECL Western Blotting Substrate	Pierce	Cat# 32106
FBS	Sigma	Cat# 12103C-100ML
DMEM	Invitrogen	Cat# 11995-073
Penicillin/Streptomycin	ThermoFisher	Cat# 15140122
Beta-mercaptoethanol	Sigma	Cat# M3148
4x Laemmli Sample Buffer	Bio-rad	Cat# 161077
Critical Commercial Assays		
Click-iT EdU Alexa Fluor 488 Imaging Kit	Life Technologies	Cat# C10337
Total RNA Purification Plus Micro Kit	Norgen	Cat# 48500
Qubit RNA HS assay kit	ThermoFisher	Cat# Q32852
Ribo-Zero Gold rRNA Removal kit	Illumina	Cat# MRZG12324
SureSelect Strand Specific RNA library prep kit	Agilent	Cat# G9691A
Superscript III Reverse Transcriptase Kit	Invitrogen	Cat# 18080-044
SYBR Green master mix	Bio-Rad	Cat# 170-8884
Deposited Data		
FUCCI embryos RNA-sequencing data	This paper	GEO: GSE118851
Mendeley dataset: E2F- EdU- pH3 IHC/IF staining wide-field and confocal microscopic images	This paper	https://doi.org/10.17632/5r6kf37zd4.1
Experimental Models: Cell Lines		
Mouse: NIH 3T3 cells	ATCC	Cat# CRL-1658
Mouse: *E2f1*$^{-/-}$;*E2f2*$^{-/-}$;*E2f3*$^{-/-}$ (TKO) Mouse embryonic fibroblasts	Wu et al., 2001	N/A
Experimental Models: Organisms/Strains		
Mouse: E2F4$^{myc/myc}$, mixed background (FVB/NT, 129v/Sv, C57BL/6NT)	This paper	N/A
Mouse: E2F8$^{myc/myc}$, mixed background (FVB/NT, 129v/Sv, C57BL/6NT)	This paper	N/A

(*Continued on next page*)

Please cite this article in press as: Cuitiño et al., Two Distinct E2F Transcriptional Modules Drive Cell Cycles and Differentiation, Cell Reports (2019), https://doi.org/10.1016/j.celrep.2019.05.004

Continued

REAGENT or RESOURCE	SOURCE	IDENTIFIER
Mouse: Wild type, mixed background (FVB/NT, 129v/Sv, C57BL/6NT)	This paper	N/A
Mouse: FUCCI, mixed background (FVB/NT, 129v/Sv, C57BL/6NT)	Sakaue-Sawano et al., 2008	N/A
Mouse: Lgr5-EGFP-IRES-creERT2 (also known as B6.129P2-Lgr5tm1(cre/ERT2)Cle/J)	The Jackson laboratory	JAX stock #008875
Oligonucleotides		
For primers used for $4^{myc/myc}$ and $8^{myc/myc}$ mouse genotyping, see Table S4	This paper	N/A
For primers used for RT-qPCR, see Table S4	This paper	N/A
Recombinant DNA		
pBABE-Hygro	Morgenstern and Land, 1990	Addgene plasmid #1765
pBABE-Hygro-E2F3a	Kent et al., 2017	N/A
pBABE-Hygro-E2F3b	Kent et al., 2017	N/A
Software and Algorithms		
STAR v2.5.3	Dobin et al., 2013	https://github.com/alexdobin/STAR
Samtools v0.1.18	Li et al., 2009	http://samtools.sourceforge.net/
HTSeq-count v.0.8.0	Anders et al., 2015	https://htseq.readthedocs.io/en/release_0.11.1/
DESeq2 v1.16.1	Love et al., 2014	http://bioconductor.org/packages/release/bioc/html/DESeq2.html
DiRE	Gotea and Ovcharenko, 2008	https://dire.dcode.org
ImageJ	Schneider et al., 2012	https://imagej.nih.gov/ij/plugins/cell-counter.html
NIS-Elements	Nikon	https://www.microscope.healthcare.nikon.com/downloads
Olympus FV10-ASW software (Ver. 4.02)	OLYMPUS	http://www.olympus-lifescience.com/en

CONTACT FOR REAGENT AND RESOURCE SHARING

Further information and requests for resources and reagents should be directed to and will be fulfilled by the Lead Contact, Gustavo Leone (leoneg@musc.edu).

EXPERIMENTAL MODEL AND SUBJECT DETAILS

Mouse models and care

FUCCI mice were purchased from RIKEN BioResource Research Center (Sakaue-Sawano et al., 2008). The *E2f4*$^{myc/myc}$ and *E2f8*$^{myc/myc}$were generated using standard homologous recombination cloning techniques. Briefly, *E2f4* and *E2f8* specific probes were used to screen CHORI-29 NOD/LtJ and 129Sv/Ev bacterial artificial chromosome library, respectively. A 10.2 kb fragment of *E2f4* spanning exon 1-7 was isolated from CH29-532D08, and a 12.8 kb fragment of *E2f8* containing exon 1-6 was isolated from RPCI-22-539-P23. In-Fusion cloning kit (Clontech Company) was used to generate *E2f4*- and *E2f8*-targeting vectors, and confirmed by direct sequencing. Targeting vectors were linearized with NotI and purified by Phenol–chloroform extraction. Standard homologous recombination techniques were used to introduce the targeted allele into mouse embryonic stem cells (ESCs) and generate chimeric mice by the Genetically Engineered Mouse Modeling Core Shared Resources at Ohio State University Comprehensive Cancer Center (OSUCCC). Correct recombination was screened and confirmed by Southern blots using the indicated restriction enzymes and probes in Figure S2C-F. The wild-type and transgenic band are also noted. ESCs with transgene were expanded and then injected into donor blastocysts that were then implanted into pseudopregnant females. Offspring from chimeric mice were bred to *Sox2-Cre* (Hayashi et al., 2002) (purchased from Jackson Laboratory) or *ACT-FLPe* (Rodríguez et al., 2000) (purchased form Jackson Laboratory) mice to produce progeny with Myc-tagged alleles as illustrated in Figures S2C and S2D, respectively. Genotypic analysis of offspring was performed on tail DNA by standard PCR techniques using allele-specific primers listed in Table S4. FUCCI mice, *E2f4*$^{myc/myc}$, *E2F8*$^{myc/myc}$ and wild-type controls were maintained on a mixed background (FVB/NT, 129v/Sv, C57BL/6NT). The Lgr5-EGFP-IRES-creERT2 were purchased from The Jackson Laboratories (Barker et al., 2007). Mouse usage was approved by the Institutional Animal Care and Use Committee at the Ohio State University and Medical University of South Carolina.

Mice were housed under normal husbandry conditions (five or less animals per cage) in a vivarium with a 12-hour light/dark cycle. Adult tissues were collected from mice at 6-16 weeks of age. To obtain embryos, female mice were cohabitated with male mice and checked daily for copulatory plugs. The presence of a copulatory plug was deemed embryonic day 0.5 (E0.5). We collected adult and embryonic tissues from both male and female randomly to eliminate sex differences, except for reproductive organs.

Cell culture

All cell lines were cultured in Dulbecco's Modified Eagle Medium (DMEM) (Invitrogen; 11995-073) supplemented with 10% Fetal Bovine Serum (Sigma; 12103C-100ML) and 1% Penicillin/Streptomycin (ThermoFisher; 15140122) in a humidified incubator at 37°C and 5% CO_2. Mouse embryonic fibroblasts (MEFs) were isolated from E13.5 embryos from corresponding genetic groups and immortalized using the 3T3 method (Xu, 2005). E2F3A and E2F3B were overexpressed in NIH 3T3 mouse cell line by transduction in retroviral vector pBABE-Hygro (Addgene; 1765) containing the sequence for murine *E2f3a* or *E2f3b*. Information about the sex of the NIH 3T3 cells was not available as cells were purchased from ATCC (see KRT).

METHOD DETAILS

5–ethynyl–2′–deoxyuridine (EdU) injection

Five mg/kg body weight of EdU (Life Technologies; C10337) dissolved in sterile phosphate-buffered saline (PBS) was intraperitoneally injected 30 min or 60 min before the mice were euthanized, for embryonic and adult mice respectively.

Tissue preparation and histology

Tissue used for histology was collected from corresponding genetic groups and fixed with 10% pH-buffered formalin (Fisher Scientific; 23-245-685) for 48 h at room temperature, embedded in paraffin and cut into 4 μm sections for histological staining.

Immunostaining

Immunostaining was performed on a Bond Rx (Leica) or Ventana discovery ultra (Roche) autostainer as per manufacturer's instructions as previously described (Campton et al., 2015; Pitarresi et al., 2016). Primary antibodies and dilutions used in this study were as follows: Ki-67 (Abcam; ab16667, 1:200), pH3-S10 (Millipore; 06-570, 1:250), FoxM1 (Santa Cruz; sc-502, 1:800), E2f3a (Millipore; 05-551, 1:100) and Myc-tag (Cell Signaling Technology; 2278, 1:100). EdU staining was performed following the manufacturer's protocol (Life Technologies; C10337).

Image acquisition and processing

Wide-field micrographs were collected using a Nikon Eclipse Ni-U microscope with a DS-Ri2 (immunohistochemistry) or a DS-Qi2 (immunofluorescence) camera and NIS-Elements Advanced Research software. Confocal micrographs were collected using the Olympus FV 1000 Filter Confocal system in Campus Microscopy & Imaging Facility (CMIF) at the Ohio State University. Images were processed for presentation using Olympus FV10-ASW software (Ver. 4.02). For visualization purposes only, background autofluorescence and non-specific staining were corrected by adjusting the intensity range using Look-Up Tables (non-destructive modifications) so to primarily display pixels representing specific signal. Tissues of *E2f3a*$^{-/-}$ and wild-type mice were used to aid in these corrections in the case of E2F3A and MYC-tag immunostaining, respectively. ImageJ (https://imagej.net/Welcome) was used for manual quantification of immunostaining on multichannel fluorescent images.

Flow cytometry

Fucci embryos from each time point were collected and minced using scissors in ice-cold disassociation solution (0.1 mg/ml DNase I (Sigma; 4716728001), 0.25% trypsin (ThermoFisher; 25200056)). After brief pipetting, the cell suspension was incubated at 37°C for 20 min and then transferred to a new dish with disassociation solution for another 15 min. Cells were transferred to Dulbecco's Modified Eagle Medium (DMEM) (Invitrogen; 11995-073) with 10% FBS (Sigma; 12103C-100ML) and then centrifuged for 10 min at 1200 RPM. The pellet was resuspended in 1X phosphate buffered saline Calcium/Magnesium free sorting buffer with 0.1mg/ml DNase I, and finally transferred to a 5 mL BD Falcon tube with cell strainer cap (35 um). The filtered suspension was diluted to a final concentration of 10 million cells/ml. The diluted suspension was then sorted using a Becton Dickinson FACS Aria III instrument equipped with FACSDiva software version 6.1.3 at the Analytical Cytometry Shared Resource Facility at The Ohio State University. Flow-sorted cells were immediately spun down at 4°C and resuspended in Buffer RL (Norgen; 48500).

RNA-sequencing

Total RNA was purified using the Norgen Bioteck Total RNA Purification Plus Micro Kit (Norgen; 48500) and concentrations were measured using the Qubit RNA HS assay kit (ThermoFisher; Q32852). An average of 200-600 ng of total RNA was obtained per sample. RNA quality was assessed using an Agilent Bioanalyzer RNA 6000 Nano chip (Agilent; 5067-1511) and RIN numbers ranged from 6-10 except for the P4 population which was consistently lower (3-5). rRNA was removed from purified total RNA using Ribo-Zero Gold rRNA Removal kit (Illumina; MRZG12324). 200 ng of rRNA-depleted RNA was used for the construction of the library using the SureSelect Strand Specific RNA library prep kit (Agilent; G9691A) according to the manufacturer's instruction, except for omitting

Please cite this article in press as: Cuitiño et al., Two Distinct E2F Transcriptional Modules Drive Cell Cycles and Differentiation, Cell Reports (2019), https://doi.org/10.1016/j.celrep.2019.05.004

the purification step before fragmentation. Barcoded libraries were pooled and sequenced using an Illumina HiSeq4000, producing paired-end 150 bp reads. RNA-seq paired-end reads were aligned to the mm10 mouse reference genome (GRCm38 release 89) using the ultrafast universal RNA-seq aligner (STAR v2.5.3)(Dobin et al., 2013). Genewise counts were assessed with HTSeq-count v.0.8.0(Anders et al., 2015). DESeq2 v1.16.1(Love et al., 2014) was used to compute regularized log-2 levels of gene expression and estimate differentially expressed genes. Distant regulatory elements (DiRE) analysis was conducted using the DiRE website (https://dire.dcode.org) (Gotea and Ovcharenko, 2008) searching evolutionary conserved 5′ untranslated regions (5′UTR) and promoter regions for genes on the mouse (mm9) genome.

Chromatin Immunoprecipitation Sequencing (ChIP-seq) hits

The ChIP-seq hits shown in the heatmaps in Figure 1 and Figure S1 were identified in previous publications (Kent et al., 2017; Kent et al., 2016; Oki et al., 2018; Santos et al., 2015; Westendorp et al., 2012). *E2f1*, *E2f3a* and *E2f3b* hits (Kent et al., 2017) were found ± 2kb distance from the transcription starting site (TSS) in mouse embryonic fibroblasts (MEFs). *E2f4* hits (Oki et al., 2018) were found ± 1kb distance from the TSS in MEFs. *E2f7* (Westendorp et al., 2012) and *E2f8 (Kent et al., 2016)* hits were found in a region defined as 5kb upstream and 2kb downstream of the TSS in HeLa cells.

Real-time PCR (RT-PCR)

One hundred ng total RNA prepared from flow sorted cells as described above was used for first strand cDNA synthesis with Superscript III Reverse Transcriptase Kit (Invitrogen; 18080-044) following the manufacturer's protocol. Quantitative PCR (qPCR) was performed using SYBR Green master mix (Bio-Rad; 170-8884) with Applied Biosystems StepOnePlus Real-Time PCR System. Samples were analyzed in triplicate and the relative expression levels of genes were calculated with the $2-\Delta\Delta Ct$ method. *Gapdh* mRNA level was used for normalization. Primers used for qPCR are listed in Table S4.

Western blot

Protein was isolated from NIH 3T3 cells, MEFs or Embryos using Radioimmunoprecipitation assay buffer (RIPA buffer). Equal amount of protein from each genetic group was loaded in SDS-PAGE and transferred to PVDF membrane (Millipore). Membranes were blocked using 5% fat-free milk in TBS and incubated in primary antibody diluted in 5% fat-free milk-TBS containing 0.1% Tween-20: rabbit polyclonal E2F3 (Santa Cruz; sc-878, 1:2000), mouse monoclonal E2F3 (Millipore; 05-551, 1:2000), rabbit monoclonal MYC (Cell Signaling Technology; 2278, 1:1000), mouse monoclonal E2F8 (Santa Cruz; sc-514064, 1:500), mouse monoclonal E2F4 (Millipore; MABE160, 1:1000), hFAB Rhodamine anti-GAPDH (BIO-RAD; 12004168, 1:3000) and hFAB Rhodamine anti-β-Actin Primary Antibody (BIO-RAD; 12004164, 1:1000). The membranes were incubated in HRP-conjugated anti-rabbit (GE; NA934, 1:2000) or mouse (Jackson ImmunoResearch Laboratories; 115-035-174, 115-035-071, 1:2000) secondary antibodies and detected using BIO-RAD ChemiDoc Imaging Systems or X-ray film.

QUANTIFICATION AND STATISTICAL ANALYSIS

No statistical analysis was used to predetermine sample size and the suitability of statistical approaches. Quantifications were performed from at least two independent experiments and quantified blindly. Sample sizes, statistical tests and p values are indicated in the text, figures and figure legends. All the quantitative data are presented in mean ± SD.

Image analysis/Immunostaining quantification

Cell nuclei from E13.5 intestinal epithelium were automatically segmented based on DAPI staining using a deep learning based approach (Van Valen et al., 2016). Each cell nucleus was then associated to one or several markers by using the fluorescence intensity levels (see Figure S6A). For each pairwise combination of markers involving E2F4 (E2F4 and EdU, E2F4 and pH3 and E2F3A and E2F4), three images for n = 2 mice were analyzed. For any other pairwise combination of markers (E2F3A and EdU, E2F3A and pH3, E2F8 and EdU, E2F8 and pH3 and E2F3A and E2F8), two to four images for n = 3 mice were analyzed.

Nuclear Segmentation

Initially, epithelial cells and their contours from five images were manually annotated to build a training dataset. These images were normalized by subtracting at each pixel the average intensity measured in a 113x113 window (the size of the imaging field) and dividing the intensity at each pixel by the median intensity. The imaging field was chosen to be larger than any cell. Five deep learning classifiers were then trained by using the convolutional neural network architecture shown in Figure S6B. A first set of 15 images were segmented with the trained classifiers. These segmentations were manually corrected and added to the previous training dataset to train again five deep-learning classifiers. The rest of the images used in the study were segmented with these deep classifiers and manually corrected.

Binary identification

Image intensity was first normalized for each image and each channel to correct for intensity variations. At each pixel and for each channel independently, the average intensity measured in a 113x113 window was subtracted, and the result was divided by the median intensity over the channel.

Thresholding strategies were then used to characterize the markers presence. Normalized images were preliminary filtered with a Gaussian blurring (radius = 1 pixel) to decrease sensitivity to noise. Depending on the modality (confocal or wide-field microscopy) and the association between markers in the images, different thresholding methods were applied to the images (Table S5), including the Triangle (Zack et al., 1977), Huang (Huang and Wang, 1995), Li (Li and Tam, 1998) and Mean (Glasbey, 1993) thresholding methods as implemented in the Auto Threshold plugin in Fiji (Schindelin et al., 2012).

Finally, positive cells for each marker were defined according to the proportion between the thresholded area and the nuclear area. In order to identify pH3-punctate cells in which only a small area of the nucleus corresponding to small dots in the image is above the threshold, cell nuclei with more than 5% but less than 90% of their area belonging to the pH3 thresholded image were considered as pH3-punctate positive. pH3-diffuse positive cells show a very clear diffuse pattern over the nucleus. Consequently, cell nuclei with more than 90% of their area belonging to the pH3 thresholded image were considered as pH3-diffuse. EdU-punctate cells show a larger labeled area than pH3-punctate cells. Therefore, cell nuclei with at least 10% but less than 65% (resp. 50%) in confocal images (resp. wide-field images) of their area belonging to the EdU thresholded image were considered as EdU-punctate positive. Cell nuclei with more than 65% in confocal images, or more than 50% in wide-field images, of their area belonging to the EdU thresholded image were considered as EdU-diffuse. Wide-field images have a lower spatial resolution than confocal images because of the out-of-focus light, resulting in blurrier structures observed in the images. For this reason, a smaller area is required to identify EdU-diffuse positive cells in wide-field images versus in confocal images. E2F3A, E2F8, E2F4 and DAPI channels show regular patterns and were considered as positive when the thresholded area was superior to 25% of the nuclear area. It has to be noted that E2F3A, E2F8, E2F4, EdU-punctate, EdU-diffuse, pH3-punctate and pH3-diffuse positive cells also have to be identified as DAPI positive cells to be taken into account in the analysis. The results of the quantification for each individual image are shown in Table S2.

The results of this automated quantification were consistent with the results from manual quantification of the staining done on the same image sets using the cell counter tool of imageJ (https://imagej.nih.gov/ij/plugins/cell-counter.html) (see Table S2).

Temporal expression

From the intensity measured in E2F3A, E2F8 and E2F4 positive cells, temporal evolution of protein concentration was estimated for each combination of markers based on three fundamental assumptions:

1) temporal evolution of protein concentration is similar in all observed cells,
2) time is proportional to the observed number of cells in the images,
3) E2F3A, E2F8 and E2F4 levels are concave downward parabolas, i.e., they increase from 0 to their maximum and then decrease from this maximum to 0.

As proliferation in intestinal epithelium is asynchronous, the first assumption is true. The second assumption is verified as the number of images is sufficiently high to observe all cell cycle phases. The third assumption originates from the knowledge that cell cycle-regulated proteins accumulate over time in specific phases and are then degraded, resulting in a downward parabola shape for protein concentration.

Four levels of intensity were considered for E2F3A, E2F8 and E2F4. For each image, levels 1 through 3 of intensity range from the minimum to the maximum average intensity measured in the nuclei of positive cells. The level 0 of intensity corresponds to negative cells. The temporal evolution of E2F3A, E2F8 and E2F4 protein concentration is inferred from histograms describing the number of cells for each intensity level (see Figure S6G, S6H and Table S3). Let us define $h(I_1 = x, I_2 = y)$ as the number of cells for which the intensity of marker 1 is equal to x and the intensity of marker 2 is equal to y. The time period $T(I_1 = x, I_2 = y)$ for which the intensity of marker 1 is equal to x and the intensity of marker 2 is equal to y is defined as:

$$T(I_1 = x, I_2 = y) = \frac{h(I_1 = x, I_2 = y)}{\sum_{x=0}^{3} \sum_{y=0}^{3} h(I_1 = x, I_2 = y)}.$$

The sequence of the time periods $h(I_1 = x, I_2 = y)$ for the different intensities is defined to hold the third assumption true and is illustrated in the histograms as arrows. The circle outlined in black corresponds to the sequence's first step. In addition, some elements of the histograms are grouped together (histogram elements circled in Figure S6G) to take into account all cells while keeping the third assumption true. As we know that pH3-diffuse cells correspond to mitosis, pH3 data were used as cell cycle reference to register the other data for each E2F protein concentration. Additionally, the histograms obtained for E2F4 and pH3 demonstrate that one single parabola for E2F4 concentration over the cell cycle is not consistent with the data. Consequently, E2F4 has to be expressed in two distinct waves of protein expression over the cell cycle.

The estimated temporal dynamics for E2F3A and E2F8, and E2F3A and E2F4 are shown in Figure S6G and S6H. The average temporal dynamics of E2F3A over these two sets of data is shown along the temporal dynamics of E2F8 and E2F4 in Figure 7A.

DATA AND SOFTWARE AVAILABILITY

RNA-sequencing data has been deposited in NCBI Gene Expression Omnibus (GEO) database with accession number GEO: GSE118851. All confocal and wide-field micrographs used for analysis and quantification of the immunostaining of E2Fs and cell cycle markers have been deposited in Mendeley data (https://doi.org/10.17632/5r6kf37zd4.1).

Cell Reports, Volume *27*

Supplemental Information

Two Distinct E2F Transcriptional Modules

Drive Cell Cycles and Differentiation

Maria C. Cuitiño, Thierry Pécot, Daokun Sun, Raleigh Kladney, Takayuki Okano-Uchida, Neelam Shinde, Resham Saeed, Antonio J. Perez-Castro, Amy Webb, Tom Liu, Soo In Bae, Linda Clijsters, Nicholas Selner, Vincenzo Coppola, Cynthia Timmers, Michael C. Ostrowski, Michele Pagano, and Gustavo Leone

Figure S1

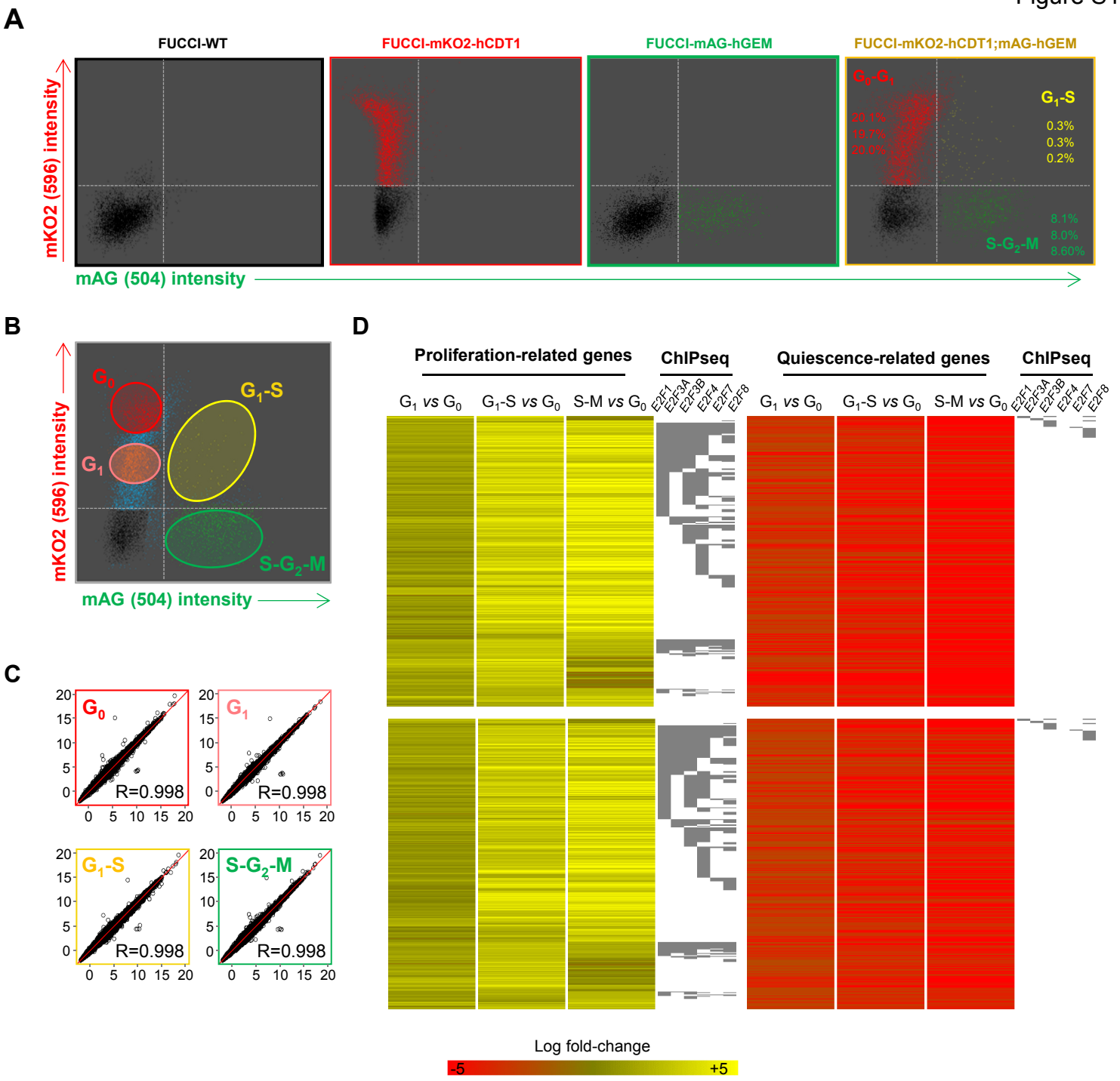
A
FUCCI-WT
FUCCI-mKO2-hCDT1
FUCCI-mAG-hGEM
FUCCI-mKO2-hCDT1;mAG-hGEM
mKO2 (596) intensity
mAG (504) intensity
G0-G1
G1-S
20.1%
19.7%
20.0%
0.3%
0.3%
0.2%
8.1%
8.0%
8.60%
S-G2-M
B
G0
G1
G1-S
S-G2-M
mKO2 (596) intensity
mAG (504) intensity
C
G0
G1
G1-S
S-G2-M
R=0.998
D
Proliferation-related genes
ChIPseq
Quiescence-related genes
ChIPseq
G1 vs G0
G1-S vs G0
S-M vs G0
E2F1
E2F3A
E2F3B
E2F4
E2F7
E2F8
Log fold-change
-5
+5
E
G0 cells
G1 cells
G1-S cells
S-G2-M cells
Regularized natural values
E2f1
E2f2
E2f3a
E2f3b
E2f4
E2f5
E2f6
E2f7
E2f8
F
Quiescence-related genes
Proliferation-related genes (258)
Cyclebase (378)
267
172
86
292

Figure S1. Related to Figure 1 and Table S1. *In vivo* analysis of cell cycle dependent mRNA profiles.

(A) FACS analysis of wild type, single transgenic (*FUCCI-mKO2-hCDT1* or *FUCCI-mAG-hGEM*), and bi-transgenic (*FUCCI-mKO2-hCDT1;mAG-hGEM*) embryos at embryonic day 13.5 (E13.5). The numbers on the far right represent the percentage of G_0+G_1 (pooled), G_1-S and S-G_2-M cells isolated from three different embryos.

(B) FACS analysis of bi-transgenic (*mKO2-hCDT1;mAG-hGEM*) FUCCI embryos at E13.5. Gated cell populations based on cell cycle phase are indicated (G_0, G_1, G_1-S and S-G_2-M).

(C) Correlation of regularized log-2 levels of gene expression, as measured by RNA-Sequencing (RNA-seq), between two replicates of the G_0, G_1, G_1-S and S-G_2-M cell populations. R, Pearson correlation coefficient.

(D) Heat maps of the log-2 fold-change values for differentially expressed genes in the cycling (G_1, G_1-S and S-G_2-M) and quiescent (G_0) cell populations at E10.5 (n=2 embryos, top) and E11.5 (n=1 embryo, bottom). E2F target genes as identified by Chromatin Immunoprecipitation (ChIP) experiments are indicated on the right of each heat map.

(E) Gene expression analysis of E2F family members in the FUCCI cell populations shown as log regularized counts (absolute levels), as measured by RNA-Seq. Each bar represents an E13.5 FUCCI embryo from an independent experiment.

(F) Venn diagram displaying the overlap between the quiescence and proliferation-related genes in the FUCCI cell populations and those available on the Cyclebase database.

Figure S2

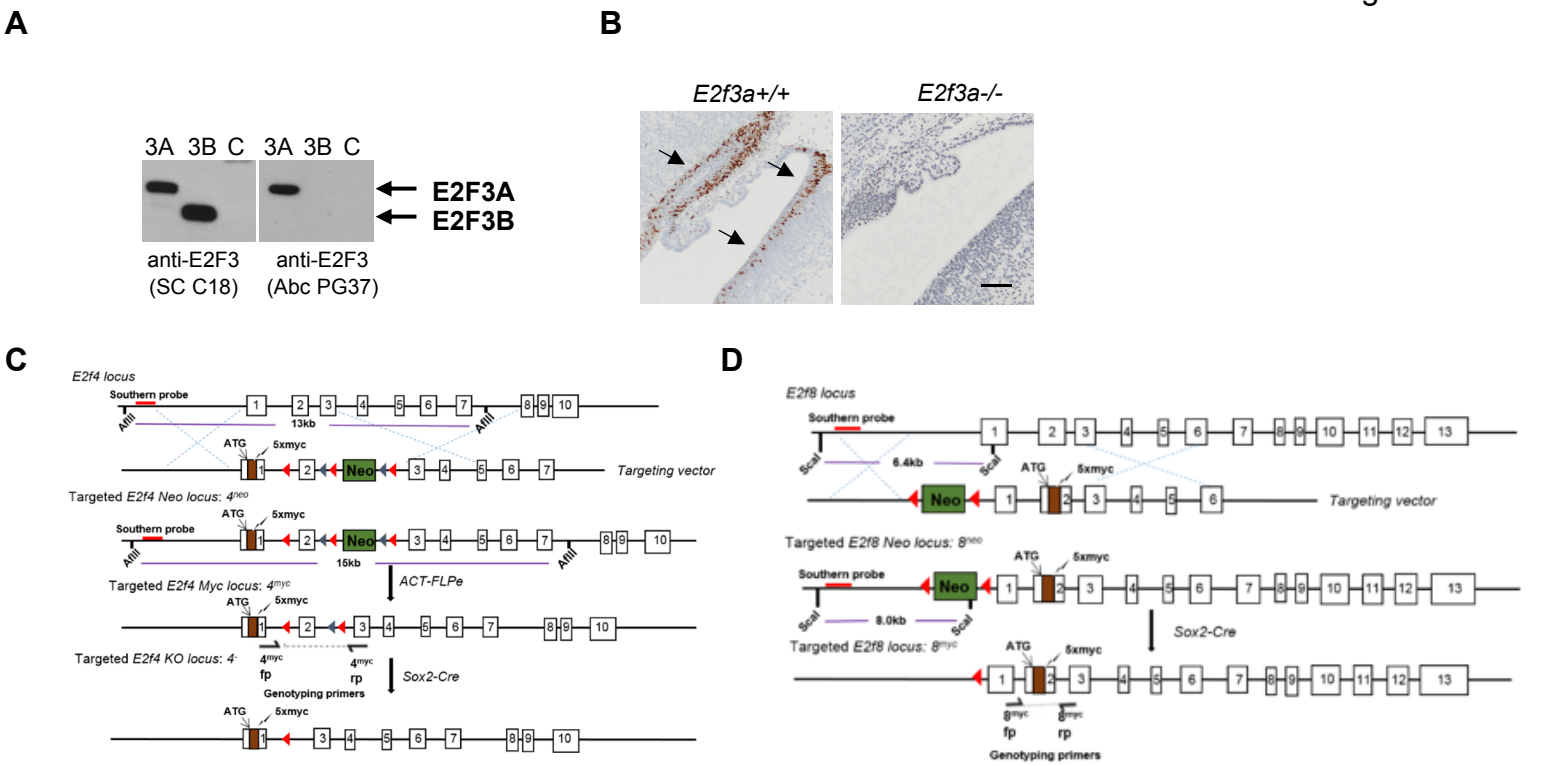

Genotype	Expected	Observed
E2f4$^{+/+}$	22.8	22
E2f4$^{myc/+}$	45.5	48
E2f4$^{myc/myc}$	22.8	21
Total		91

Genotype	Expected	Observed
E2f7$^{+/+}$*E2f8*$^{+/+}$	5.1	5
E2f7$^{+/+}$*E2f8*$^{myc/+}$	10.3	12
E2f7$^{+/+}$*E2f8*$^{myc/myc}$	5.1	2
E2f7$^{+/-}$*E2f8*$^{+/+}$	10.3	6
E2f7$^{+/-}$*E2f8*$^{myc/+}$	20.5	22
E2f7$^{+/-}$*E2f8*$^{myc/myc}$	10.3	11
E2f7$^{-/-}$*E2f8*$^{+/+}$	5.1	6
E2f7$^{-/-}$*E2f8*$^{myc/+}$	10.3	14
E2f7$^{-/-}$*E2f8*$^{myc/myc}$	5.1	4
Total		82

Figure S2. Related to Figure 2. Generation of E2F3A, E2F4, and E2F8 specific reagents.

(A) Immunoblots of protein lysates from NIH3T3 cells overexpressing *E2f3a* (3A), *E2f3b* (3B) were probed with an E2F3 antibody detecting both E2F3A and E2F3B (SC C-18, left) or an antibody specific for E2F3A (Abc PG37, right). *E2f1*$^{-/-}$;*E2f2*$^{-/-}$;*E2f3*$^{-/-}$ (TKO) mouse embryonic fibroblasts (MEFs) were used as a control (C).

(B) E2F3A immunohistochemistry (IHC) on brain sections of *E2f3a*$^{+/+}$ and *E2f3a*$^{-/-}$ E13.5 embryos using the E2F3A specific antibody (PG37). The lack of immunolabelling on the *E2f3a*$^{-/-}$ tissue demonstrates the specificity of the E2F3A antibody.

(C) Diagram of the mouse *E2f4* locus, targeting vector, and targeted *E2f4* locus prior to and after deletion of the neomycin (Neo) cassette (green) and exon 2 in germ line using ACT-FLPe and Sox2-Cre, respectively. The 5×MYC tag (brown) was inserted after the ATG. Dashed lines indicate homologous recombination between targeting vector and endogenous *E2f4* locus. The red line represents the Southern probe used to test embryonic stem (ES) cell clones after AflII digestion. The blue and red triangle represents the FRT and loxP site, respectively.

(D) Diagram of the mouse *E2f8* locus, targeting vector, and targeted *E2f8* locus prior to and after deletion of the neomycin (Neo) cassette (green) in germ line using Sox2-Cre. The 5×MYC tag (brown) was inserted after the ATG. Dashed lines indicate homologous recombination between targeting vector and endogenous *E2f8* locus. The red line represents the Southern probe used to test embryonic stem (ES) cell clones after ScaI digestion. The red triangle represents the loxP site.

(E) Southern blotting for the *E2f4*$^{+}$ and *E2f4*^{neo} alleles in ES cells.

(F) Southern blotting for the *E2f8*$^{+}$ and *E2f8*^{Neo} alleles in ES cells.

(G) PCR genotyping of DNA from *E2f4*$^{myc/+}$, *E2f4*$^{+/+}$, and *E2f4*$^{+/-}$ mice using primers flanking the FRT, loxP site and the exon2 shown in Figure S2C. The *E2f4*^{myc} (858 bp), *E2f4*$^{+}$ (734 bp) and *E2f4*$^{-}$ (400 bp) bands are noted.

(H) PCR genotyping of DNA from *E2f8*$^{myc/+}$, *E2f8*$^{myc/myc}$, and *E2f8*$^{+/+}$ mice using primers flanking the Myc tag site shown in Figure S2D. The *E2f8*^{myc} (520 bp) and *E2f8*$^{+}$ (350 bp) bands are noted.

(I) Western blotting of lysates from *E2f4*$^{+/+}$, *E2f4*$^{myc/+}$, *E2f4*$^{myc/myc}$ and *E2f4*$^{-/-}$ E13.5 embryos using anti-E2F4 and anti-MYC antibody. The main MYC-E2F4 (~70 kDa) and E2F4 (~55 kDa) bands are noted. GAPDH is used as a loading control.

(J) Western blotting of lysates from *E2f8*$^{+/+}$, *E2f8*$^{myc/+}$, and *E2f8*$^{myc/myc}$ E13.5 embryos using anti-E2F8 and anti-Myc antibodies. The main E2F8 (~110 kDa) and MYC-E2F8 (~130 kDa) bands are noted. β-Actin is used as a loading control.

Figure S2. Continued

(K) E2F4 IHC on the small intestine of *E2f4*$^{+/+}$ and *E2f4*$^{myc/myc}$ mice using MYC antibody. The lack of immunolabelling on the *E2f4*$^{+/+}$ intestine demonstrates the specificity of the MYC antibody.

(L) E2F8 IHC on the small intestine of *E2f8*$^{myc/myc}$ and *E2f8*$^{+/+}$ mice using MYC antibody. The lack of immunolabelling on the *E2f8*$^{+/+}$ intestine demonstrates the specificity of the MYC antibody.

(M) Pictures of *E2f4*$^{myc/myc}$ and *E2f4*$^{+/+}$ mice.

(N) Genotypes of day 21 offspring originating from *E2f4*$^{myc/+}$ intercrosses.

(O) Pictures of *E2f8*$^{+/+}$ and *E2f8*$^{myc/myc}$ mice.

(P) Genotypes of day 0 offspring originating from *E2f7*$^{+/-}$ *E2f8*$^{myc/+}$ intercrosses. Scale bars: 200 μm.

Figure S3

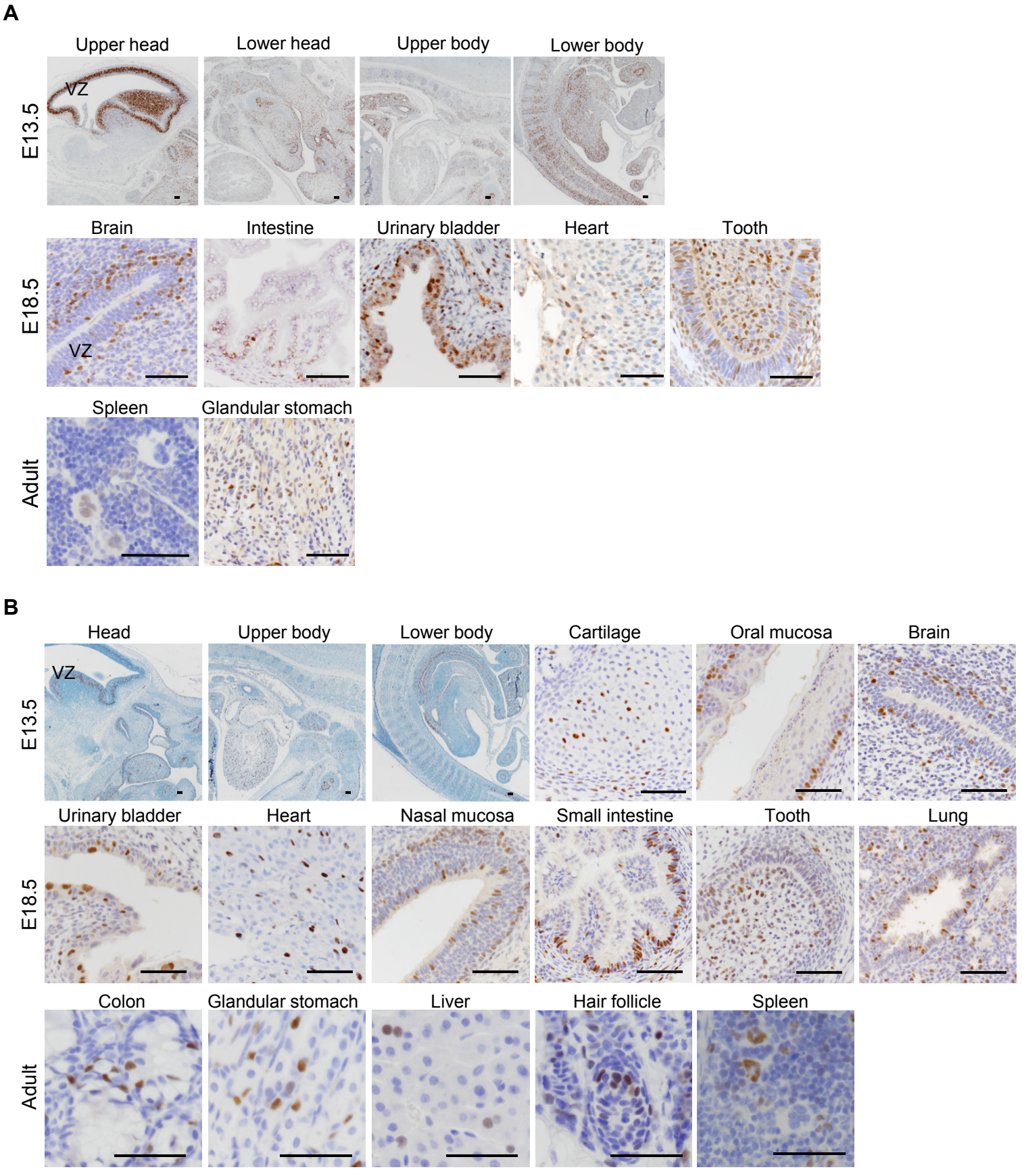
A
Upper head
Lower head
Upper body
Lower body
E13.5
VZ
Brain
Intestine
Urinary bladder
Heart
Tooth
E18.5
VZ
Spleen
Glandular stomach
Adult
B
Head
Upper body
Lower body
Cartilage
Oral mucosa
Brain
E13.5
VZ
Urinary bladder
Heart
Nasal mucosa
Small intestine
Tooth
Lung
E18.5
Colon
Glandular stomach
Liver
Hair follicle
Spleen
Adult

Figure S3. Related to Figure 2. E2F3A and E2F8 expression in embryonic and adult tissues.

(A) E2F3A IHC in tissues of wild type embryos and adult mice. The level of proliferation of the tissues included in this figure as evidenced by Ki67 IHC is provided in Figure S5A.

(B) E2F8 IHC in tissues of *E2f8*$^{myc/myc}$ embryos and adult mice using MYC antibody. The level of proliferation of the tissues included in this figure as evidenced by Ki67 IHC is provided in Figure S5A. VZ, ventricular zone. Scale bars: 200 μm.

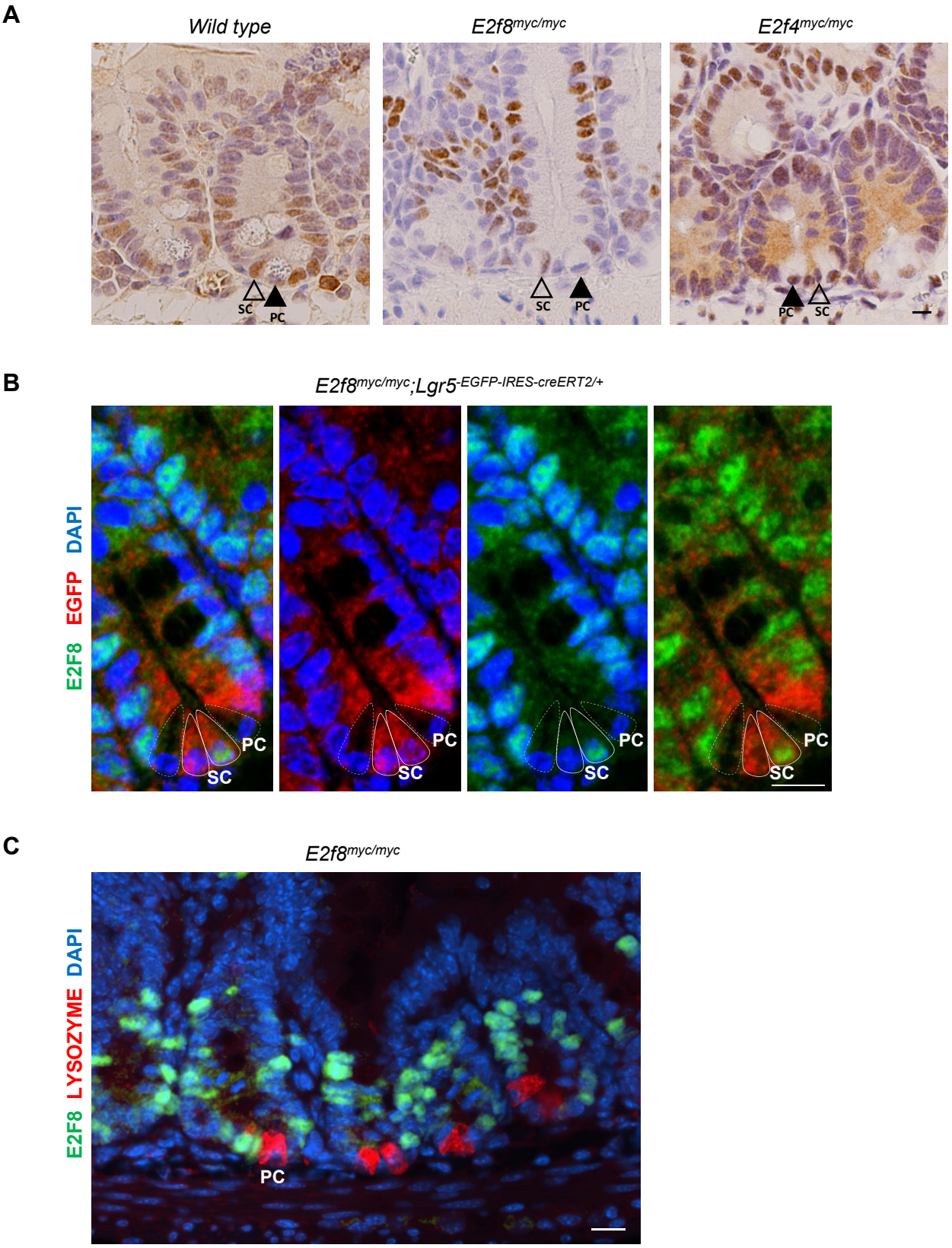
A
Wild type
E2f8myc/myc
E2f4myc/myc
SC
PC
B
E2f8myc/myc;Lgr5-EGFP-IRES-creERT2/+
E2F8 EGFP DAPI
PC
SC
C
E2f8myc/myc
E2F8 LYSOZYME DAPI
PC

Figure S4. Related to Figure 2. E2F3A, E2F8 and E2F4 expression in intestinal cell types.

(A) E2F3A, E2F8 and E2F4 IHC (left to right) on the small intestine of adult mice with indicated genotypes. SC, stem cell; PC, Paneth cell.

(B) Immunofluorescence of E2F8 (green) and LGR5-EGFP (red) on the small intestine of adult mice with the indicated genotype. DAPI counterstain (blue). Left, composite image; middle-left, red and blue channels; middle-right, green and blue channels; right, green and red channels. SC, stem cell (solid lines); PC, Paneth Cell (dashed lines).

(C) Immunofluorescence of E2F8 (green) and Paneth cell marker lysozyme (red) on the small intestine of adult $E2f8^{myc/myc}$ mice. DAPI counterstain (blue). PC, Paneth Cell. Scale bars: (A) and (C) 20 μm, (B) 10 μm.

Figure S5

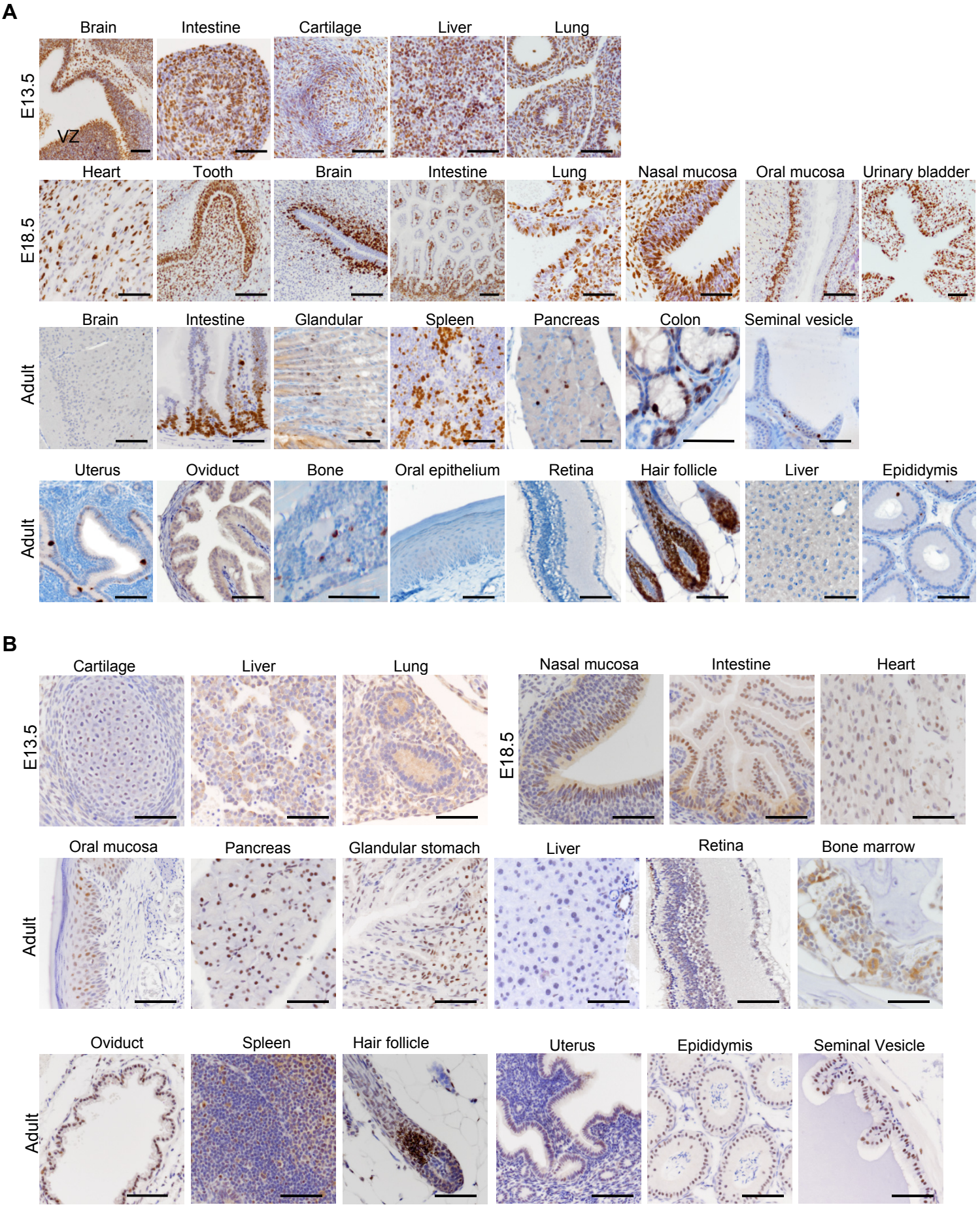
A
Brain
Intestine
Cartilage
Liver
Lung
E13.5
VZ
Heart
Tooth
Brain
Intestine
Lung
Nasal mucosa
Oral mucosa
Urinary bladder
E18.5
Brain
Intestine
Glandular
Spleen
Pancreas
Colon
Seminal vesicle
Adult
Uterus
Oviduct
Bone
Oral epithelium
Retina
Hair follicle
Liver
Epididymis
Adult
B
Cartilage
Liver
Lung
E13.5
Nasal mucosa
Intestine
Heart
E18.5
Oral mucosa
Pancreas
Glandular stomach
Liver
Retina
Bone marrow
Adult
Oviduct
Spleen
Hair follicle
Uterus
Epididymis
Seminal Vesicle
Adult

Figure S5. Related to Figure 2. Ki67 and E2F4 expression in embryonic and adult tissues.

(A) Analysis of cellular proliferation by Ki67 IHC in tissues of wild type embryos and adult mice.

(B) E2F4 IHC in tissues of *E2f4*$^{myc/myc}$ embryos and adult mice using MYC antibody. The level of proliferation of the tissues included in this figure as evidenced by Ki67 IHC is provided in (A). VZ, ventricular zone. Scale bars: 200 μm.

A

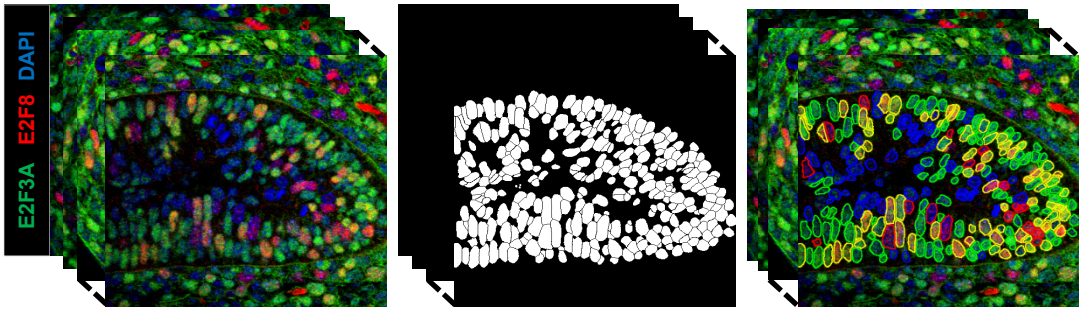

1) Images from intestinal epithelium

2) Deep learning based nuclear segmentation

3) Binary identification

B

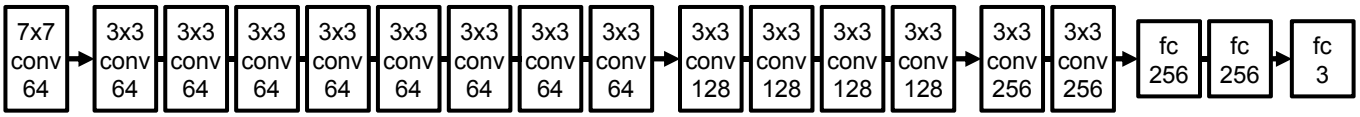

C

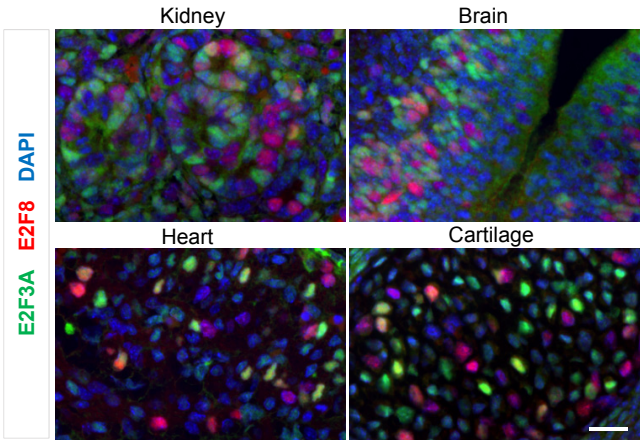

D

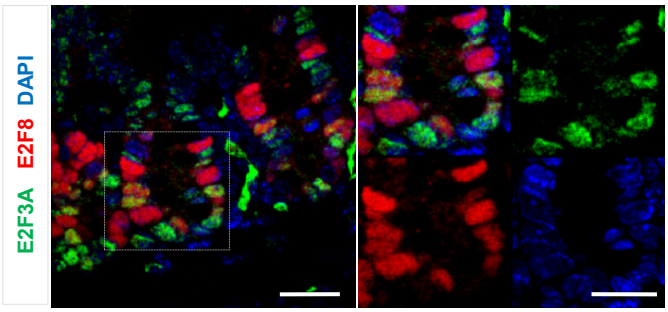

E

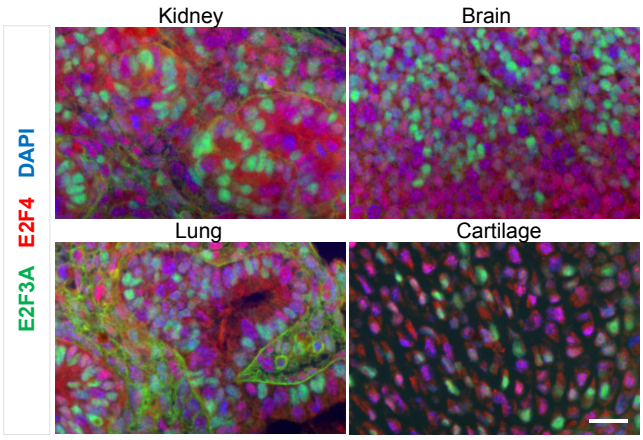

F

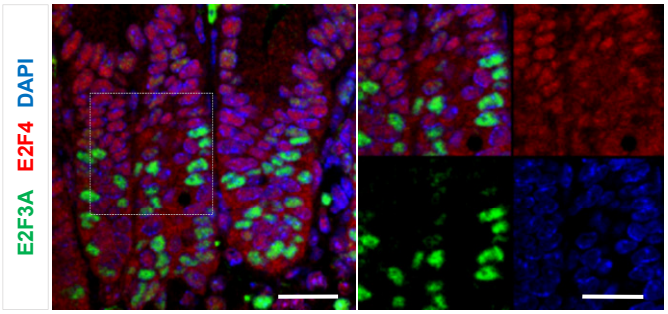

G

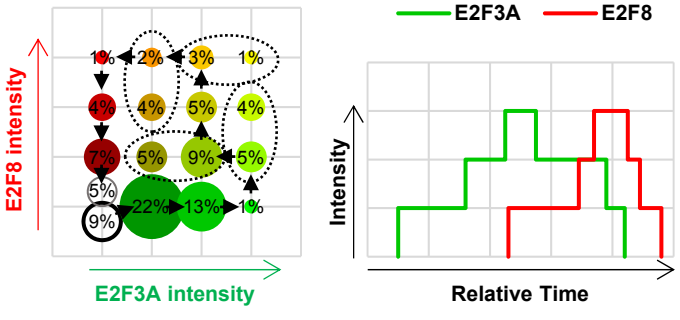

H

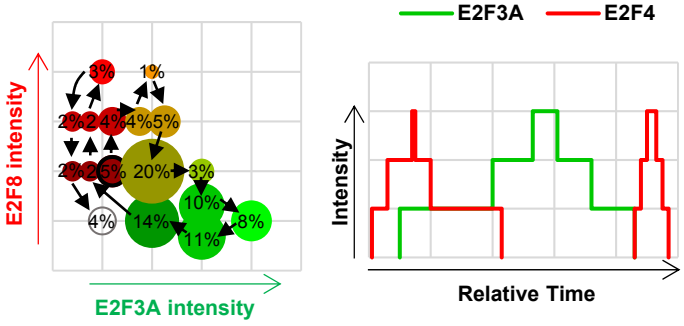

Figure S6. Related to Figure 4, Table S2 and Table S3. Distinct expression of E2F3A, E2F8 and E2F4.

(A) Image quantification pipeline.

(B) Convolutional neural network architecture used for the deep learning based nuclear segmentation. 7x7 conv 64 stands for a convolutional layer of 64 7x7 filters. Fc 256 stands for a fully connected 256x256 layer. Each arrow corresponds to a max pooling layer. At each convolutional or fully connected layer, a batch normalization and a rectified linear unit activation are processed, except for the last layer where a softmax activation is processed.

(C) E2F3A (green) and E2F8 (red) immunofluorescence on indicated tissues of *E2f8*$^{myc/myc}$ E13.5 embryos. DAPI counterstain (blue).

(D) E2F3A (green) and E2F8 (red) immunofluorescence on the small intestine of *E2f8*$^{myc/myc}$ adult mice. DAPI counterstain (blue).

(E) E2F3A (green) and E2F4 (red) immunofluorescence on indicated tissues of *E2f4*$^{myc/myc}$ E13.5 embryos. DAPI counterstain (blue).

(F) E2F3A (green) and E2F4 (red) immunofluorescence on the small intestine of *E2f4*$^{myc/myc}$ adult mice. DAPI counterstain (blue). E2F8 and E2F4 were detected using MYC antibody. The images in (D) and (F) are confocal micrographs. Scale bars: 20 μm.

(G-H) Left: 2D histograms depicting the distribution of the normalized nuclear intensity of E2F3A and E2F8 (G) and E2F3A and E2F4 (H). Circle size is proportional to the percentage of nuclei. The arrows illustrate how the temporal expression curves are defined. The circle outlined in black corresponds to the sequence's first step. Right: estimated temporal dynamics from the histograms in (G) and (H) (see methods for details).

Figure S7

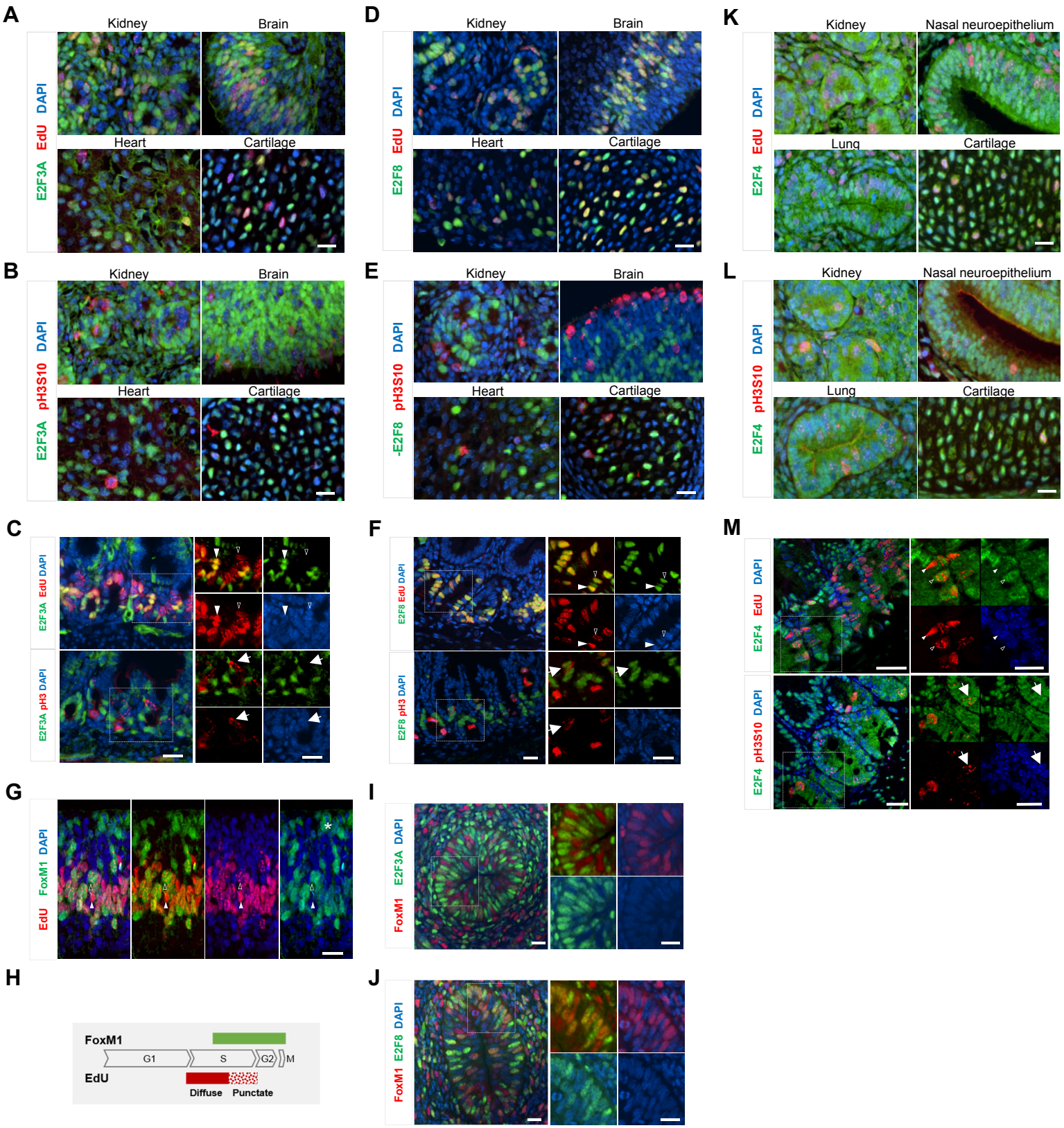
A
Kidney
Brain
Heart
Cartilage
DAPI
EdU
E2F3A
B
Kidney
Brain
Heart
Cartilage
DAPI
pH3S10
E2F3A
C
E2F3A EdU DAPI
E2F3A pH3 DAPI
D
Kidney
Brain
Heart
Cartilage
DAPI
EdU
E2F8
E
Kidney
Brain
Heart
Cartilage
DAPI
pH3S10
-E2F8
F
E2F8 EdU DAPI
E2F8 pH3 DAPI
G
EdU
FoxM1
DAPI
H
FoxM1
G1
S
G2
M
EdU
Diffuse
Punctate
I
FoxM1
E2F3A
DAPI
J
FoxM1
E2F8
DAPI
K
Kidney
Nasal neuroepithelium
Lung
Cartilage
DAPI
EdU
E2F4
L
Kidney
Nasal neuroepithelium
Lung
Cartilage
DAPI
pH3S10
E2F4
M
E2F4 EdU DAPI
E2F4 pH3S10 DAPI

Figure S7. Related to Figure 6 and Table S2. E2F3A, E2F8 and E2F4 expression in the cell cycle.

(A) EdU (red) and E2F3A (green) immunofluorescence on indicated tissues of wild type E13.5 embryos. DAPI counterstain (blue).

(B) pH3 (red) and E2F3A (green) immunofluorescence on indicate tissues of wild type E13.5 embryos. DAPI counterstain (blue).

(C) EdU (red) and E2F3A (green) (top), and pH3 (red) and E2F3A (green) (bottom) immunofluorescence on the small intestine of wild type adult mice. DAPI counterstain (blue).

(D) EdU (red) and E2F8 (green) immunofluorescence on indicated tissues of *E2f8*$^{myc/myc}$ E13.5 embryos. DAPI counterstain (blue).

(E) pH3 (red) and E2F8 (green) immunofluorescence on indicated tissues of *E2f8*$^{myc/myc}$ E13.5 embryos. DAPI counterstain (blue).

(F) EdU (red) and E2F8 (green) (top), and pH3 (red) and E2F8 (green) (bottom) immunofluorescence on the small intestine of *E2f8*$^{myc/myc}$ adult mice. DAPI counterstain (blue).

(G) EdU (red) and FoxM1 (green) immunofluorescence on the ventricular zone of the brain of wild type E13.5 embryos. DAPI counterstain (blue).

(H) Schematic of the proposed distinct temporal pattern of staining of FoxM1 displayed in (G).

(I) FoxM1 (red) and E2F3A (green) immunofluorescence on the intestine of wild type E13.5 embryos. DAPI counterstain (blue).

(J) FoxM1 (red) and E2F8 (green) immunofluorescence on the intestine of wild type E13.5 embryos. DAPI counterstain (blue).

(K) EdU (red) and E2F4 (green) immunofluorescence on indicated tissues of *E2f4*$^{myc/myc}$ E13.5 embryos. DAPI counterstain (blue).

(L) pH3 (red) and E2F4 (green) immunofluorescence on indicated tissues of *E2f4*$^{myc/myc}$ E13.5 embryos. DAPI counterstain (blue).

(M) EdU (red) and E2F4 (green) (top), and pH3 (red) and E2F4 (green) (bottom) on the small intestine of *E2f4*$^{myc/myc}$ adult mice.

E2F8 and E2F4 were detected using MYC antibody. In (C), (F), (I), (J), and (M), color-split images of the boxed area are shown on right panels; top-left, red and green channels; top-right, red and blue channels; bottom-left, green and blue channels; bottom-right, blue channel. In (G), composite and color-split images are shown; left, composite; middle-left, green and red channels; middle-right, red and blue channels; right, green and blue channels. Solid arrowheads: EdU-Diffuse. Open arrowheads: EdU-Punctate. Arrows: pH3 Punctate. Asterisks: mitosis. Scale bars: 20 μm.